Chemical Geology 401 (2015) 111–125

Contents lists available at ScienceDirect

Chemical Geology

journal homepage: www.elsevier.com/locate/chemgeo

# Chemical and Pb isotope composition of olivine-hosted melt inclusions from the Hannuoba basalts, North China Craton: Implications for petrogenesis and mantle source

Sheng-Ping Qian [a,b], Zhong-Yuan Ren [a,*], Le Zhang [a], Lu-Bing Hong [a,b], Jian-Qiang Liu [a,b]

[a] State Key Laboratory of Isotope Geochemistry, Guangzhou Institute of Geochemistry, Chinese Academy of Sciences, Guangzhou 510640, China
[b] University of Chinese Academy of Sciences, Beijing 100049, China

ARTICLE INFO

*Article history:*
Received 4 June 2013
Received in revised form 6 January 2015
Accepted 18 February 2015
Available online 27 February 2015

Editor: L. Reisberg

*Keywords:*
Cenozoic basalts
Melt inclusion
Recycled crust
Pyroxenite
North China Craton

ABSTRACT

Melt inclusions and their host olivine provide unique information about the nature, distribution and scale of mantle source heterogeneity. We present the first analyses of the chemical and Pb isotope compositions of melt inclusions and their host olivine from the Cenozoic Hannuoba basalts, North China Craton, which contains coexisting suites of alkali and tholeiitic basalts. There is limited variation in major and trace element composition, but significant Pb isotopic variation, in the tholeiitic samples. This contrasts with the substantial variation in major and trace elements, but limited Pb isotopic variation, in the alkali basalt samples. Based on the results of the major- and trace-element modeling, the compositional variation of the alkali basalts may be primarily attributed to garnet pyroxenite melting, with only a small input from garnet peridotite melts. The garnet–pyroxenite component involved in the genesis of the alkali basalts, of metasomatic origin, may have formed in the lithosphere. The wide range of isotopic composition of the tholeiitic basalts and remarkably limited variability of major and trace element composition is argued to be characteristic of the source region, which is a mixture of peridotite with small amounts of pyroxenite transformed from recycled ancient oceanic crust and sediment. The presence of recycled oceanic crust in the mantle source and the low–velocity anomaly observed beneath the Taihang Mountains, located 50 km to the southeast of the Hannuoba region, supports a plume model for their origin.



## 1. Introduction

The assessment of the nature and distribution of mantle source components is pivotal to understanding the origin of intraplate magmatism and the internal structure of the Earth's mantle (Zindler and Hart, 1986; Gurenko et al., 2009). Trace element and isotopic studies of erupted lavas from oceanic and continental intraplate settings have indicated that the Earth's mantle is heterogeneous (Zindler and Hart, 1986; Hofmann, 1997; Saal et al., 1998; Pilet et al., 2011). Recycled oceanic crust and sediments (Hofmann, 1997; Rehkamper and Hofmann, 1997; Eisele et al., 2002; Ren et al., 2005, 2006, 2009; Sobolev et al., 2007; Rapp et al., 2008), delaminated subcontinental lithosphere (Arndt and Goldstein, 1989; Jull and Kelemen, 2001; Gao et al., 2004; Lustrino, 2005), and recycled metasomatized lithospheric mantle (Niu and O'Hara, 2003; Workman et al., 2004; Pilet et al., 2011) have all been proposed as explanations for the enriched geochemical characteristics of some erupted lavas. Compared with oceanic intraplate basalts whose geochemistry and petrology have been investigated intensively and comprehensively (e.g. Zindler and Hart, 1986; Hofmann, 1997), the origin of continental intraplate basalts is not always well understood (Farmer, 2003; Timm et al., 2010).

Cenozoic basalts are widespread in the North China Craton (NCC), Mongolia, and northeastern China, and are viewed as representative of intraplate basalts in a continental setting (Basu et al., 1991). Numerous petrological and geochemical studies that have been carried out over the past two decades (Song et al., 1990; Zhi et al., 1990; Basu et al., 1991; Xu et al., 2005, 2012a; Tang et al., 2006; Choi et al., 2008; Chen et al., 2009; Zhang et al., 2009; Wang et al., 2011; Zeng et al., 2011; Hong et al., 2013; Sakuyama et al., 2013) show that the Cenozoic basalts in the NCC have ocean island basalt (OIB)-type trace element compositions (e.g. enriched in large ion lithophile elements (LILE), displaying light rare-earth element (LREE) enrichment, $(La/Sm)_{PM} > 1$, and positive Nb and Ta anomalies). These findings imply the presence of components in their mantle source that are considerably enriched in incompatible trace elements compared to the depleted mid-ocean ridge

* Corresponding author at: Guangzhou Institute of Geochemistry, Chinese Academy of Sciences, 510640 Wushan, Guangzhou, China. Tel.: +86 20 85292969; fax: +86 20 85290261.
*E-mail address:* zyren@gig.ac.cn (Z.-Y. Ren).

http://dx.doi.org/10.1016/j.chemgeo.2015.02.018
0009-2541/

basalt (MORB)-type asthenospheric mantle. It is generally accepted that the geochemical characteristics of these basalts can be attributed to the mixing of a depleted mantle component and an EMI-like component (Song et al., 1990; Zhi et al., 1990; Basu et al., 1991; Xu et al., 2005; Tang et al., 2006; Choi et al., 2008). However, the origin and the nature of the depleted and enriched mantle components and the processes that enrich the mantle are still hotly debated.

Traditionally, the variability of chemical and isotopic compositions observed in intraplate basalts has been presumed to reflect that of their mantle source (Zindler and Hart, 1986). Melt inclusions that are extremely chemically and isotopically heterogeneous have recently been found in single-rock samples and even in single olivine grains, implying that melt inclusions can provide increased resolution of mantle source heterogeneities (Sobolev and Shimizu, 1993; Gurenko and Chaussidona, 1995; Saal et al., 1998; Ren et al., 2005; Maclennan, 2008). The aggregation of melts migrating toward the surface and mixing in the crust can considerably reduce the diversity of bulk compositions and consequently often obscure the primary characteristics of the mantle sources (Saal et al., 1998; Danyushevsky et al., 2000; Sobolev et al., 2000; Ren et al., 2005; Kamenetsky et al., 2006, 2012; Maclennan, 2008). Melt inclusions have proven to be a valuable tool for defining the compositions of pre-aggregated melts, assessing the nature of their mantle sources, and investigating the physico-chemical evolution of magmatic systems (Saal et al., 1998; Sobolev et al., 2000; Ren et al., 2005; Kamenetsky et al., 2006, 2012; Maclennan, 2008).

In this paper, we present the first analyses of elemental and Pb isotopic compositions of melt inclusions and their host olivines from the Cenozoic Hannuoba basalts (including co-existing alkali and tholeiitic basalts) in the northern NCC. In combination with analyses of the whole-rock compositions, these data are used to: (1) identify the mantle source lithology; (2) understand the nature and origin of the depleted and enriched components in the mantle source; (3) determine the petrogenesis of the Cenozoic basalts, thereby constraining the evolution of the mantle lithosphere beneath the NCC.

## 2. Geological setting and petrographic characteristics

The NCC, regarded as one of the world's oldest cratons, preserves continental crustal relics dating back to 3.8 Ga (Liu et al., 1992). Tectonically, the NCC is bound to the north by the late Paleozoic to Mesozoic Central Asian Orogenic belt, to the west by the Qilian Orogenic belt, and to the south by the Qinling–Dabie–Sulu Orogenic belt (Zhao et al., 2001). The basement of the NCC is partitioned into the Eastern Block, the Western Block and the Trans-North China Belt between the two, based on geochronological and geochemical data, and the metamorphic P–T–t path (the pressure (P)–temperature (T)–time (t) path of a metamorphic rock) of the basement rocks (Zhao et al., 2001; Fig. 1a). The final amalgamation of the NCC occurred at 1.8 Ga following the collision of the Eastern and Western Blocks, leading to the closure of an ancient ocean basin (Zhao et al., 2001). The NCC remained stable until Carboniferous–Triassic times when weak magmatic activity occurred. Since the late Mesozoic, intensive tectono-thermal reactivation, as evidenced by lithospheric thinning, extensive magmatic activity and the formation of sedimentary basins, occurred mainly in the eastern part of the NCC (Menzies et al., 1993; Xu, 2001; Zhang et al., 2003; Wu et al., 2005; Tang et al., 2008, 2013).

Cenozoic basalts are widely distributed in eastern China (Basu et al., 1991). The Hannuoba basaltic plateau, located along the northern margin of the Trans-North China Belt, has drawn widespread attention for its size, the occurrence of interlayered tholeiites and alkali basalts and the numerous mantle and crustal xenoliths in the alkali basalts (Fig. 1a) (Zhi et al., 1990). These basalts have been K–Ar dated at 14–22 Ma (Liu, 1992). The co-existence of tholeiites and alkali basalts in the Hannuoba basaltic plateau testifies to a great geochemical diversity that is not otherwise typical of the NCC.

All samples analyzed here, including 8 tholeiites and 24 alkali basalts, were collected from Zhenhutai and Damaping, which are located northwest of Zhangjiakou in the Hebei province (Fig. 1b). The tholeiitic basalts contain rare euhedral to subhedral olivine phenocrysts. The groundmass is generally microcrystalline, consisting of plagioclase, clinopyroxene, olivine, and opaque minerals, in addition to glass. Melt inclusions that have a round to elliptical shape and contain microcryst filaments are found in some of the olivine phenocrysts. Their size ranges from several to 80 μm. Melt inclusions occur individually or in small clusters, but not along fractures, and can be considered primary. The alkali basalts are fine-grained, with rare and small olivine phenocrysts. The groundmass is microcrystalline and is comprised of plagioclase, clinopyroxene, olivine, and opaque minerals. Melt inclusions occur in some olivine and consist of glass, microlites and vapor bubbles.

## 3. Analytical methods

The samples were cut into thin slabs, and the central parts that were free of weathering and alteration were selected. The fresh samples were split into small chips, cleaned several times in distilled water in an ultrasonic tank and dried prior to powdering for chemical analysis. All of the analyses were performed at the State Key Laboratory of Isotope Geochemistry, Guangzhou Institute of Geochemistry, Chinese Academy of Sciences (GIG-CAS).

Whole-rock major elements were determined on fused glass disks using a Rigaku ZSX-100e X-ray fluorescence spectrometer (XRF) according to the analytical methods reported by Goto and Tatsumi (1996). Analytical precision was better than 5% for the majority of major elements. Trace element analyses were carried out using a Perkin-Elmer ELAN 6000 inductively coupled plasma mass spectrometer (ICP-MS), following the methods reported by Liu et al. (1996). Analytical uncertainty for most trace elements was better than 5% based on repeated analyses of U.S.G.S. standards BHVO-2, AGV-1 and AGV-2. The results of standards for the major and trace element analyses are listed in Table S4.

To determine the chemical composition of glass inclusions, it is almost always preferable to analyze a homogeneous glass rather than a mixture of various crystalline phases and residual glass. Therefore, slowly cooled melt inclusions containing mixtures of crystals and glass require reheating and quenching prior to analysis (Danyushevsky et al., 2000; Ren et al., 2005). To homogenize olivine-hosted melt inclusions, a 1 atm gas-mixing furnace was used to heat olivine grains to 1,250 °C at the quartz–fayalite–magnetite (QFM) buffer. Olivine grains were rapidly lifted to the top of the furnace and quenched after being heated for 10 min. A more detailed procedure of this process has been described by Ren et al. (2005). Major and minor elements of the melt inclusions and host olivine were determined with an electron microprobe JEOL JXA-8100 Superprobe, following the procedures reported by Wang and Gaetani (2008) for the melt inclusions, and by Sobolev et al. (2007) for olivine. Olivine was analyzed at an accelerating voltage of 20 kV, a 300 nA beam current and a focused beam (2 μm), while melt inclusions were measured at an accelerating voltage of 15 kV, a 20 nA beam current and a focused beam (3 μm). Before and after each batch analysis, an internal olivine and an internal glass standard (JB-2) were measured to detect instrumental drift (Ren et al., 2004). The analytical results indicate that uncertainties for the olivine standard ($2\sigma$, $n = 30$) were better than 0.16% for $SiO_2$ and MgO, 0.38% for FeO, 1.35% for MnO and NiO, and 4.43% for CaO, while uncertainties for JB-2 ($2\sigma$, $n = 25$) were better than 0.12% for $SiO_2$, 0.32% for $TiO_2$, $Al_2O_3$ and CaO, 0.65% for FeO, MgO and $Na_2O$, and 2.29, 9.93 and 11.90% for $K_2O$, MnO, and $P_2O_5$, respectively (Table S4).

In situ Pb isotope compositions of melt inclusions were determined using a Neptune plus MC-ICP-MS and RESOlution M-50 laser ablation system (with a wavelength of 193-nm, spot size of 45-μm, energy of 80-mJ, attenuate value of 25%, repetition rate of 3-Hz, and an integration

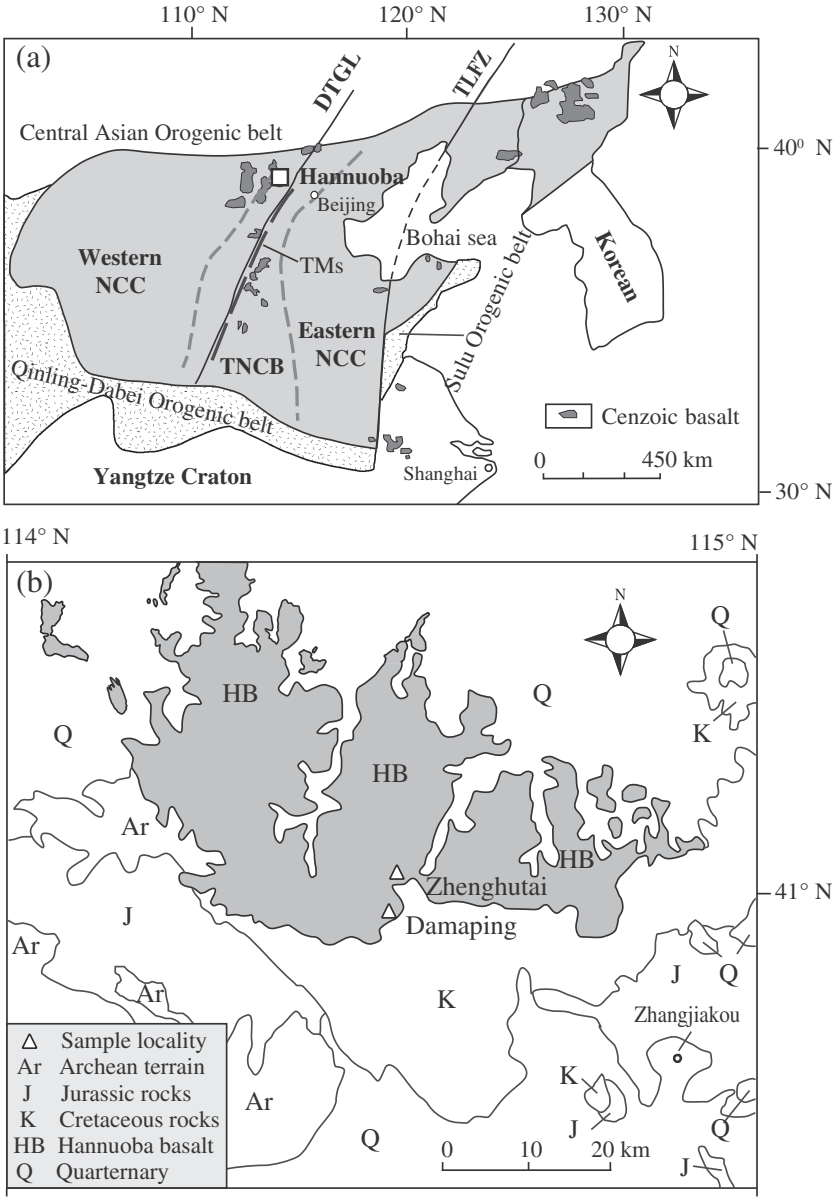


**Fig. 1.** (a) Simplified tectonic map of the North China Craton (NCC) and the location of the study area; note that the NCC is cut by two major geological and geophysical linear zones, the Tan-Lu fault zone (TLFZ) to the east and the Daxinganlin–Taihangshan gravity lineament (DTGL) to the west (modified after Xu et al., 2005). The Cenozoic Hannuoba basalts (white square) occur at the northern margin of the NCC. The distribution of Cenozoic basalts in the NCC is from Xu et al. (2005). TNCB, Trans-North China Belt. TMs, Taihang Mountains. (b) Distribution of Cenozoic basalts at Hannuoba and sampling localities. Open triangles represent sampling localities.

time of 0.262-s). Samples were analyzed using a JET sample cone and an X skimmer cone. Before analysis, the sample surfaces were cleaned in an ultrasonic bath with dilute $HNO_3$ (<1%) and Milli-Q water for 10–15 min, rinsed several times with distilled water and dried with a nitrogen gas gun. The international reference materials NKT-1G and BHVO-2G were selected as the intensities of their $^{208}Pb$ peaks resemble those of the melt inclusions. These standards were measured in turn to evaluate the accuracy of the instrument prior to analysis (Zhang et al., 2014). Before and after every five analyses, an internal glass standard (BHVO-2G) was measured to detect instrumental drift. The average value of the internal glass standard was 2.0542 for $^{208}Pb/^{206}Pb$, and 0.8335 for $^{207}Pb/^{206}Pb$. Analytical uncertainties (2σ, n = 34) for the internal glass standard were better than 0.22% for $^{208}Pb/^{206}Pb$ and 0.36% for $^{207}Pb/^{206}Pb$, while accuracies were better than 0.09% for $^{208}Pb/^{206}Pb$, and 0.12% for $^{207}Pb/^{206}Pb$ (Table S4).

## 4. Results

### 4.1. Whole rock geochemistry

Thirty-two Hannuoba basalt samples were analyzed for major and trace element composition (Tables 1 and 2). On the total alkali vs silica (TAS) diagram (Le Bas et al., 1986), 8 samples plot well within the basalt field, while the other 24 samples can be classified as trachybasalt or basanite (Fig. 2). The CIPW-normative calculation further indicates that 24 samples contain normative nepheline (Ne), whereas the remaining eight samples contain normative olivine (Ol) and normative hypersthene (Hy) (Table 1). Here the more general classification of alkali basalts and tholeiite (Macdonald and Katsura, 1964) is adopted in view of the fact that the samples plot in the alkaline and sub-alkaline series fields of the TAS diagram, respectively (Fig. 2).

**Table 1**
Major element composition of the Hannuoba basalts.

| Rock | Tholeiites | | | | | | | | Alkali basalts | | | | | | | |
|---|---|---|---|---|---|---|---|---|---|---|---|---|---|---|---|---|
| Sample | D-1 | D-4 | D-6 | D-10 | D-18 | D-19 | D-20 | D-21 | D-2 | D-3 | D-5 | D-7 | D-8 | D-9 | D-11 | D-12 |
| $SiO_2$ | 49.00 | 49.76 | 50.16 | 49.23 | 50.28 | 50.51 | 49.80 | 51.06 | 44.46 | 44.44 | 44.39 | 43.94 | 44.13 | 44.34 | 44.13 | 44.40 |
| $TiO_2$ | 1.98 | 1.83 | 1.92 | 1.82 | 1.91 | 1.94 | 1.88 | 1.87 | 2.38 | 2.62 | 2.45 | 2.51 | 2.37 | 2.44 | 2.55 | 2.78 |
| $Al_2O_3$ | 14.07 | 14.34 | 14.22 | 14.10 | 14.18 | 14.18 | 14.14 | 14.50 | 13.05 | 13.38 | 13.33 | 13.18 | 12.98 | 13.27 | 13.19 | 13.18 |
| $(Fe_2O_3)_T$ | 12.52 | 11.28 | 12.04 | 11.31 | 11.81 | 12.02 | 11.53 | 11.60 | 13.26 | 13.43 | 13.28 | 13.30 | 13.15 | 13.25 | 13.32 | 13.37 |
| MnO | 0.14 | 0.13 | 0.14 | 0.14 | 0.15 | 0.15 | 0.14 | 0.14 | 0.17 | 0.16 | 0.17 | 0.16 | 0.17 | 0.17 | 0.16 | 0.15 |
| MgO | 6.00 | 7.66 | 7.23 | 8.21 | 6.96 | 6.95 | 7.56 | 6.85 | 10.16 | 9.20 | 9.18 | 9.11 | 10.23 | 9.14 | 8.83 | 8.16 |
| CaO | 8.71 | 8.07 | 8.37 | 8.05 | 9.02 | 8.90 | 8.18 | 8.40 | 9.44 | 8.62 | 9.36 | 8.97 | 8.95 | 9.11 | 8.80 | 8.61 |
| $Na_2O$ | 3.20 | 2.94 | 3.23 | 2.93 | 2.99 | 3.00 | 3.11 | 3.14 | 2.78 | 3.61 | 3.40 | 3.33 | 2.92 | 3.65 | 3.52 | 3.60 |
| $K_2O$ | 0.98 | 1.11 | 1.18 | 1.11 | 0.69 | 0.81 | 1.17 | 1.17 | 1.43 | 1.37 | 1.49 | 1.68 | 1.80 | 1.65 | 2.17 | 2.11 |
| $P_2O_5$ | 0.36 | 0.36 | 0.40 | 0.38 | 0.30 | 0.31 | 0.37 | 0.37 | 0.67 | 0.85 | 0.81 | 0.84 | 0.68 | 0.80 | 0.84 | 0.87 |
| L.O.I. | 2.77 | 2.18 | 0.75 | 2.41 | 1.34 | 0.86 | 1.78 | 0.62 | 1.85 | 2.05 | 1.86 | 2.73 | 2.32 | 1.89 | 2.20 | 2.53 |
| Total | 99.72 | 99.67 | 99.64 | 99.68 | 99.64 | 99.63 | 99.66 | 99.72 | 99.65 | 99.72 | 99.70 | 99.75 | 99.68 | 99.72 | 99.71 | 99.74 |
| Mg# | 51.6 | 60.1 | 57.2 | 61.7 | 56.7 | 56.2 | 59.3 | 56.7 | 63.0 | 60.3 | 60.6 | 60.3 | 63.3 | 60.5 | 59.5 | 57.6 |
| Fe/Mn | 71.5 | 69.2 | 69.2 | 67.2 | 63.7 | 65.5 | 67.5 | 68.2 | 62.7 | 67.4 | 63.9 | 66.2 | 63.1 | 63.2 | 66.5 | 71.1 |
| *CIPW normative minerals (vol.%)* | | | | | | | | | | | | | | | | |
| Q | 0.0 | 0.0 | 0.0 | 0.0 | 0.0 | 0.0 | 0.0 | 0.0 | 0.0 | 0.0 | 0.0 | 0.0 | 0.0 | 0.0 | 0.0 | 0.0 |
| Pl | 56.5 | 55.1 | 55.1 | 54.4 | 56.1 | 55.5 | 54.9 | 55.2 | 39.7 | 40.0 | 36.9 | 35.9 | 35.0 | 33.3 | 29.4 | 32.8 |
| Or | 7.2 | 8.0 | 8.4 | 8.0 | 5.0 | 5.7 | 8.4 | 8.2 | 10.5 | 10.0 | 10.9 | 12.3 | 13.2 | 12.0 | 15.8 | 15.4 |
| Ne | 0.0 | 0.0 | 0.0 | 0.0 | 0.0 | 0.0 | 0.0 | 0.0 | 5.8 | 8.6 | 9.4 | 9.3 | 8.0 | 11.6 | 12.4 | 10.8 |
| Di | 15.2 | 11.5 | 13.6 | 11.8 | 14.9 | 14.6 | 12.9 | 14.1 | 18.3 | 16.2 | 18.9 | 17.9 | 17.8 | 19.3 | 18.9 | 18.1 |
| Hy | 11.2 | 16.7 | 11.2 | 14.4 | 18.4 | 18.3 | 13.0 | 14.2 | 0.0 | 0.0 | 0.0 | 0.0 | 0.0 | 0.0 | 0.0 | 0.0 |
| Ol | 5.5 | 4.7 | 7.4 | 7.3 | 1.5 | 1.8 | 6.8 | 4.3 | 20.0 | 18.8 | 17.9 | 18.3 | 20.2 | 17.7 | 17.2 | 16.2 |
| Il | 2.5 | 2.3 | 2.4 | 2.3 | 2.4 | 2.4 | 2.3 | 2.3 | 3.0 | 3.3 | 3.1 | 3.2 | 3.0 | 3.1 | 3.2 | 3.5 |
| Mt | 1.1 | 1.0 | 1.0 | 1.0 | 1.0 | 1.0 | 1.0 | 1.0 | 1.2 | 1.2 | 1.2 | 1.2 | 1.2 | 1.2 | 1.2 | 1.2 |
| Ap | 0.8 | 0.8 | 0.9 | 0.9 | 0.7 | 0.7 | 0.9 | 0.8 | 1.6 | 1.9 | 1.8 | 1.9 | 1.6 | 1.8 | 1.9 | 2.0 |

| Rock | Alkali basalts | | | | | | | | | | | | | | | |
|---|---|---|---|---|---|---|---|---|---|---|---|---|---|---|---|---|
| Sample | D-13 | D-14 | D-15 | D-16 | D-17 | Z-1 | Z-2 | Z-3 | Z-4 | Z-5 | Z-6 | Z-7 | Z-8 | Z-9 | Z-10 | Z-11 | Z-12 |
| $SiO_2$ | 44.21 | 44.47 | 44.34 | 44.23 | 43.88 | 44.69 | 46.87 | 46.72 | 46.02 | 46.91 | 46.12 | 47.13 | 43.78 | 46.67 | 45.56 | 45.65 | 45.02 |
| $TiO_2$ | 2.51 | 2.53 | 2.46 | 2.39 | 2.37 | 2.57 | 2.43 | 2.41 | 2.41 | 2.41 | 2.25 | 2.46 | 2.65 | 2.22 | 2.44 | 2.42 | 2.42 |
| $Al_2O_3$ | 13.29 | 13.14 | 13.20 | 13.04 | 12.40 | 13.67 | 14.73 | 14.61 | 14.04 | 14.71 | 13.93 | 14.81 | 13.36 | 14.19 | 13.48 | 13.27 | 13.47 |
| $(Fe_2O_3)_T$ | 13.23 | 13.46 | 13.33 | 13.20 | 13.59 | 13.37 | 12.57 | 12.46 | 12.92 | 12.53 | 12.67 | 12.64 | 13.77 | 12.57 | 13.12 | 13.12 | 13.64 |
| MnO | 0.16 | 0.17 | 0.17 | 0.17 | 0.17 | 0.16 | 0.14 | 0.13 | 0.15 | 0.14 | 0.15 | 0.14 | 0.17 | 0.15 | 0.15 | 0.17 | 0.18 |
| MgO | 8.99 | 9.09 | 9.13 | 9.95 | 10.76 | 6.31 | 5.68 | 5.42 | 8.14 | 5.30 | 7.89 | 5.42 | 6.92 | 7.66 | 9.19 | 9.85 | 8.81 |
| CaO | 8.96 | 9.21 | 9.11 | 9.44 | 9.64 | 8.68 | 6.93 | 7.28 | 8.00 | 7.28 | 8.39 | 6.88 | 8.94 | 8.08 | 8.30 | 9.22 | 9.06 |
| $Na_2O$ | 3.08 | 3.48 | 3.78 | 2.89 | 2.38 | 4.49 | 4.26 | 3.76 | 3.55 | 3.95 | 3.23 | 4.42 | 4.30 | 3.84 | 2.98 | 2.54 | 3.00 |
| $K_2O$ | 2.11 | 1.77 | 1.59 | 1.51 | 1.70 | 2.36 | 2.77 | 3.10 | 1.38 | 3.18 | 2.01 | 2.86 | 1.96 | 1.87 | 1.54 | 1.65 | 1.92 |
| $P_2O_5$ | 0.83 | 0.81 | 0.80 | 0.68 | 0.63 | 1.30 | 0.83 | 0.83 | 0.68 | 0.83 | 0.66 | 0.83 | 1.32 | 0.68 | 0.57 | 0.69 | 0.84 |
| L.O.I. | 2.33 | 1.55 | 1.80 | 2.17 | 2.13 | 2.17 | 2.56 | 3.04 | 2.44 | 2.51 | 2.38 | 2.17 | 2.63 | 1.78 | 2.35 | 1.23 | 1.38 |
| Total | 99.69 | 99.69 | 99.72 | 99.67 | 99.64 | 99.78 | 99.76 | 99.76 | 99.73 | 99.75 | 99.70 | 99.76 | 99.80 | 99.71 | 99.69 | 99.83 | 99.75 |
| Mg# | 60.2 | 60.0 | 60.4 | 62.6 | 63.8 | 51.2 | 50.1 | 49.2 | 58.3 | 48.5 | 58.1 | 48.8 | 52.7 | 57.5 | 60.9 | 62.5 | 58.9 |
| Fe/Mn | 65.6 | 64.9 | 63.5 | 62.4 | 63.5 | 68.1 | 73.7 | 75.1 | 71.6 | 73.6 | 67.3 | 75.1 | 66.9 | 68.4 | 69.4 | 61.1 | 62.1 |
| *CIPW normative minerals (vol.%)* | | | | | | | | | | | | | | | | | |
| Q | 0.0 | 0.0 | 0.0 | 0.0 | 0.0 | 0.0 | 0.0 | 0.0 | 0.0 | 0.0 | 0.0 | 0.0 | 0.0 | 0.0 | 0.0 | 0.0 | 0.0 |
| Pl | 33.7 | 33.1 | 32.7 | 37.7 | 34.7 | 28.6 | 39.7 | 38.7 | 49.8 | 36.6 | 43.5 | 38.5 | 30.2 | 43.2 | 46.7 | 38.6 | 35.3 |
| Or | 15.4 | 12.8 | 11.6 | 11.1 | 12.5 | 17.0 | 19.7 | 22.1 | 10.0 | 22.6 | 14.5 | 20.2 | 14.3 | 13.4 | 11.2 | 13.2 | 13.8 |
| Ne | 9.1 | 10.8 | 12.3 | 7.2 | 6.1 | 15.6 | 9.5 | 8.0 | 3.9 | 9.5 | 5.1 | 10.4 | 14.9 | 7.2 | 3.0 | 5.3 | 8.1 |
| Di | 17.7 | 19.6 | 19.8 | 18.9 | 20.0 | 18.7 | 12.1 | 12.8 | 13.0 | 13.4 | 15.1 | 12.5 | 18.9 | 14.9 | 14.4 | 18.0 | 18.5 |
| Hy | 0.0 | 0.0 | 0.0 | 0.0 | 0.0 | 0.0 | 0.0 | 0.0 | 0.0 | 0.0 | 0.0 | 0.0 | 0.0 | 0.0 | 0.0 | 0.0 | 0.0 |
| Ol | 17.9 | 17.5 | 17.5 | 19.4 | 21.0 | 12.8 | 13.1 | 12.4 | 17.6 | 12.0 | 16.4 | 12.5 | 14.2 | 15.8 | 19.3 | 19.2 | 17.8 |
| Il | 3.2 | 3.2 | 3.1 | 3.0 | 3.0 | 3.2 | 3.0 | 3.0 | 3.0 | 3.0 | 2.8 | 3.0 | 3.4 | 2.8 | 3.1 | 3.0 | 3.4 |
| Mt | 1.2 | 1.2 | 1.2 | 1.2 | 1.2 | 1.2 | 1.1 | 1.1 | 1.1 | 1.1 | 1.1 | 1.1 | 1.2 | 1.1 | 1.2 | 1.2 | 1.2 |
| Ap | 1.9 | 1.9 | 1.8 | 1.6 | 1.5 | 2.9 | 1.9 | 1.9 | 1.6 | 1.8 | 1.5 | 1.9 | 3.0 | 1.5 | 1.3 | 1.6 | 1.9 |

Major oxides are reported in weight percent (wt.%). Mg# = molar 100 × Mg / (Mg + Fe), assuming $Fe^{2+}/Fe_{total} = 0.9$. $(Fe_2O_3)_T$ is total iron as $Fe_2O_3$. Q—quartz, Ab—albite, Or—orthoclase, Ne—nepheline, Hy—hypersthene, Ol—olivine, Il—ilmenite, Mt—magnetite, Ap—apatite.

Tholeiitic and alkali basalts can be readily distinguished on a $SiO_2$–MgO variation diagram (Fig. 3a). Generally, the alkali basalts have higher contents of $K_2O$, $TiO_2$, and $Fe_2O_3^T$ (total iron as $Fe_2O_3$, not shown) but lower contents of $SiO_2$ compared to tholeiitic basalts at a given MgO content (Fig. 3). The tholeiitic basalts have a limited range of MgO content, 6–8.3 wt.%, in contrast to the relatively wide range, 5 to 11 wt.% in alkali basalts. CaO and $CaO/Al_2O_3$ in alkali basalts decrease with falling MgO, whereas CaO and $CaO/Al_2O_3$ display no correlation with MgO for the tholeiitic basalts (Fig. 3). Both alkali and tholeiitic basalts have high Fe/Mn ratios (mostly >65, Table 1).

In general, the alkali basalts show greater enrichment of incompatible trace elements compared with the tholeiitic basalts (Table 2). The alkali basalts display a pattern of strong LREE enrichment [$(La/Yb)_N = 16.9–48.1$] and MREE/HREE differentiation [$(Sm/Yb)_N = 5.3–13.1$] (Table 2) without a Eu anomaly (Fig. 4a and b), while the tholeiites show lower LREE/HREE [$(La/Yb)_N = 6.7–10$] and less differentiation of MREE/HREE [$(Sm/Yb)_N = 3.24–4.3$] (Table 2). The alkali basalts show positive Nb and Ta anomalies but have negative Pb and K anomalies on primitive mantle normalized spidergrams (Fig. 4). Additionally, they display depletion in Hf and Ti ($Hf/Hf^* = 0.66–0.98$, $Ti/Ti^* = 0.40–0.97$) and enrichment in Sr. The trace element distribution patterns of tholeiitic basalts are different from those of the alkali basalts, and are characterized by a positive K anomaly and no significant depletion in Hf and Ti ($Hf/Hf^* = 0.78–0.90$, $Ti/Ti^* = 0.90–1.06$)

**Table 2**
Trace element composition of the Hannuoba basalts.

| Rock | Tholeiites | | | | | | | | Alkali basalts | | | | | | | |
|---|---|---|---|---|---|---|---|---|---|---|---|---|---|---|---|---|
| Sample | D-1 | D-4 | D-6 | D-10 | D-18 | D-19 | D-20 | D-21 | D-2 | D-3 | D-5 | D-7 | D-8 | D-9 | D-11 | D-12 |
| Sc (ppm) | 18 | 19 | 19 | 19 | 20 | 20 | 20 | 18 | 19 | 15 | 16 | 16 | 18 | 17 | 15 | 11 |
| Cr | 172 | 193 | 226 | 211 | 205 | 206 | 225 | 223 | 257 | 210 | 201 | 198 | 261 | 203 | 203 | 155 |
| Ni | 131 | 123 | 137 | 142 | 135 | 138 | 136 | 133 | 196 | 155 | 157 | 158 | 197 | 162 | 164 | 151 |
| Rb | 11.3 | 15.7 | 15.2 | 13.7 | 9.2 | 10.8 | 17.0 | 15.2 | 24.8 | 20.8 | 36.1 | 51.0 | 45.2 | 29.4 | 42.7 | 45.0 |
| Sr | 424 | 446 | 506 | 465 | 448 | 454 | 485 | 471 | 812 | 958 | 981 | 915 | 817 | 915 | 943 | 1066 |
| Y | 18.1 | 16.8 | 17.7 | 16.3 | 18.3 | 19.0 | 17.8 | 16.9 | 20.9 | 20.7 | 21.2 | 20.2 | 20.6 | 21.4 | 20.7 | 18.9 |
| Zr | 132 | 138 | 143 | 134 | 125 | 129 | 147 | 137 | 223 | 276 | 251 | 263 | 219 | 253 | 270 | 295 |
| Nb | 24.7 | 25.4 | 27.6 | 26.3 | 21.0 | 21.7 | 27.2 | 25.1 | 64.0 | 80.0 | 73.5 | 75.5 | 64.6 | 74.0 | 78.0 | 85.8 |
| Cs | 0.06 | 0.16 | 0.13 | 0.10 | 0.58 | 1.02 | 0.21 | 0.23 | 0.39 | 0.51 | 0.50 | 0.45 | 0.43 | 0.52 | 0.55 | 0.62 |
| Ba | 253 | 272 | 283 | 255 | 213 | 211 | 288 | 275 | 473 | 557 | 540 | 530 | 485 | 534 | 567 | 666 |
| La | 16.1 | 17.1 | 20.2 | 17.9 | 14.0 | 14.4 | 17.7 | 17.2 | 36.4 | 45.6 | 44.1 | 44.5 | 37.2 | 44.5 | 45.8 | 48.1 |
| Ce | 33.8 | 36.3 | 41.6 | 38.0 | 29.6 | 30.3 | 37.2 | 33.0 | 72.2 | 89.6 | 86.5 | 88.3 | 73.3 | 87.6 | 89.1 | 94.5 |
| Pr | 4.4 | 4.7 | 5.4 | 4.9 | 3.9 | 4.0 | 4.8 | 4.5 | 8.9 | 10.9 | 10.3 | 10.8 | 8.9 | 10.6 | 10.8 | 11.5 |
| Nd | 18.6 | 19.9 | 22.9 | 20.2 | 16.8 | 17.2 | 20.5 | 19.8 | 35.0 | 42.9 | 41.1 | 42.0 | 35.1 | 42.0 | 42.2 | 44.7 |
| Sm | 4.75 | 4.70 | 5.29 | 4.77 | 4.38 | 4.54 | 4.87 | 4.40 | 7.32 | 8.69 | 8.44 | 8.74 | 7.37 | 8.56 | 8.64 | 9.12 |
| Eu | 1.75 | 1.75 | 1.94 | 1.76 | 1.64 | 1.68 | 1.79 | 1.77 | 2.45 | 2.94 | 2.86 | 2.92 | 2.46 | 2.83 | 2.88 | 2.97 |
| Gd | 4.63 | 4.43 | 4.89 | 4.49 | 4.70 | 4.65 | 4.66 | 4.69 | 6.35 | 7.25 | 7.06 | 7.22 | 6.27 | 7.12 | 7.10 | 7.36 |
| Tb | 0.74 | 0.70 | 0.75 | 0.68 | 0.72 | 0.73 | 0.71 | 0.69 | 0.94 | 0.99 | 1.01 | 1.02 | 0.91 | 1.00 | 1.02 | 1.02 |
| Dy | 4.06 | 3.77 | 4.12 | 3.63 | 3.97 | 4.11 | 3.92 | 4.13 | 4.86 | 5.09 | 5.01 | 5.13 | 4.64 | 5.11 | 4.93 | 4.83 |
| Ho | 0.77 | 0.71 | 0.77 | 0.68 | 0.76 | 0.77 | 0.72 | 0.79 | 0.87 | 0.83 | 0.88 | 0.85 | 0.84 | 0.88 | 0.84 | 0.78 |
| Er | 1.82 | 1.69 | 1.80 | 1.62 | 1.89 | 1.89 | 1.78 | 1.98 | 2.08 | 1.89 | 2.00 | 1.92 | 1.97 | 2.07 | 1.91 | 1.66 |
| Tm | 0.25 | 0.23 | 0.25 | 0.22 | 0.26 | 0.26 | 0.25 | 0.25 | 0.26 | 0.22 | 0.24 | 0.24 | 0.26 | 0.25 | 0.23 | 0.19 |
| Yb | 1.45 | 1.36 | 1.46 | 1.29 | 1.50 | 1.52 | 1.48 | 1.52 | 1.52 | 1.24 | 1.46 | 1.34 | 1.44 | 1.42 | 1.33 | 1.02 |
| Lu | 0.22 | 0.20 | 0.21 | 0.18 | 0.22 | 0.22 | 0.19 | 0.21 | 0.21 | 0.17 | 0.19 | 0.18 | 0.20 | 0.20 | 0.17 | 0.13 |
| Hf | 3.19 | 3.14 | 3.31 | 3.02 | 3.08 | 3.16 | 3.39 | 3.28 | 4.85 | 5.85 | 5.32 | 5.75 | 4.68 | 5.44 | 5.80 | 6.35 |
| Ta | 1.28 | 1.30 | 1.47 | 1.34 | 1.11 | 1.13 | 1.39 | 1.33 | 3.37 | 4.14 | 3.90 | 3.96 | 3.35 | 3.90 | 4.08 | 4.55 |
| Pb | 2.99 | 2.58 | 2.68 | 2.13 | 2.57 | 5.68 | 3.25 | 3.06 | 3.39 | 3.75 | 4.01 | 4.01 | 3.85 | 3.88 | 3.95 | 4.31 |
| Th | 1.77 | 1.68 | 1.89 | 1.71 | 1.51 | 1.52 | 1.81 | 1.70 | 4.30 | 5.45 | 5.24 | 5.37 | 4.34 | 5.28 | 5.44 | 6.12 |
| U | 0.49 | 0.45 | 0.50 | 0.46 | 0.44 | 0.43 | 0.52 | 0.49 | 1.08 | 1.36 | 1.34 | 1.35 | 1.06 | 1.30 | 1.38 | 1.53 |
| $(La/Yb)_N$ | 7.9 | 9.0 | 9.9 | 10.0 | 6.7 | 6.8 | 8.6 | 8.1 | 17.1 | 26.3 | 21.8 | 23.8 | 18.5 | 22.5 | 24.7 | 33.7 |
| $(Sm/Yb)_N$ | 3.6 | 3.8 | 4.0 | 4.1 | 3.2 | 3.3 | 3.7 | 3.2 | 5.3 | 7.8 | 6.4 | 7.2 | 5.7 | 6.7 | 7.2 | 9.9 |
| $(La/Sm)_N$ | 3.4 | 3.6 | 3.8 | 3.8 | 3.2 | 3.2 | 3.6 | 3.9 | 5.0 | 5.2 | 5.2 | 5.1 | 5.0 | 5.2 | 5.3 | 5.3 |
| Nb/Ta | 19.2 | 19.5 | 18.8 | 19.6 | 19.0 | 19.3 | 19.6 | 18.8 | 19.0 | 19.3 | 18.8 | 19.1 | 19.3 | 19.0 | 19.1 | 18.9 |
| Zr/Hf | 41.4 | 44.1 | 43.2 | 44.5 | 40.5 | 40.8 | 43.2 | 41.8 | 45.9 | 47.2 | 47.2 | 45.7 | 46.7 | 46.6 | 46.7 | 46.4 |
| Nb/Nb* | 1.60 | 1.63 | 1.54 | 1.64 | 1.58 | 1.60 | 1.66 | 1.60 | 1.77 | 1.75 | 1.67 | 1.69 | 1.75 | 1.67 | 1.70 | 1.72 |
| Ti/Ti* | 0.98 | 0.94 | 0.90 | 0.95 | 1.03 | 1.06 | 1.03 | 1.02 | 0.85 | 0.82 | 0.77 | 0.77 | 0.86 | 0.78 | 0.82 | 0.86 |
| Hf/Hf* | 0.85 | 0.82 | 0.76 | 0.77 | 0.90 | 0.90 | 0.86 | 0.88 | 0.76 | 0.76 | 0.72 | 0.76 | 0.73 | 0.72 | 0.76 | 0.79 |
| Eu/Eu* | 1.14 | 1.17 | 1.16 | 1.16 | 1.11 | 1.12 | 1.15 | 1.19 | 1.10 | 1.13 | 1.13 | 1.12 | 1.10 | 1.11 | 1.12 | 1.11 |

| Rock | Alkali basalts | | | | | | | | | | | | | | | |
|---|---|---|---|---|---|---|---|---|---|---|---|---|---|---|---|---|
| Sample | D-13 | D-14 | D-15 | D-16 | D-17 | Z-1 | Z-2 | Z-3 | Z-4 | Z-5 | Z-6 | Z-7 | Z-8 | Z-9 | Z-10 | Z-11 | Z-12 |
| Sc | 16 | 16 | 17 | 18 | 19 | 11 | 8 | 9 | 16 | 9 | 17 | 9 | 11 | 17 | 18 | 21 | 17 |
| Cr | 224 | 194 | 207 | 252 | 293 | 114 | 77 | 80 | 205 | 92 | 200 | 87 | 120 | 205 | 258 | 243 | 163 |
| Ni | 159 | 156 | 159 | 189 | 222 | 112 | 80 | 81 | 170 | 82 | 165 | 81 | 111 | 166 | 216 | 225 | 172 |
| Rb | 39.0 | 33.6 | 32.9 | 26.1 | 28.5 | 36.8 | 40.7 | 55.5 | 32.4 | 56.3 | 56.5 | 39.5 | 34.6 | 47.1 | 33.7 | 35.6 | 31.2 |
| Sr | 964 | 964 | 914 | 777 | 1041 | 1473 | 1153 | 1176 | 912 | 1159 | 839 | 1148 | 1501 | 966 | 689 | 1104 | 1028 |
| Y | 20.8 | 20.9 | 21.4 | 21.1 | 19.9 | 23.0 | 17.1 | 17.2 | 18.6 | 17.2 | 19.1 | 17.5 | 23.4 | 19.8 | 18.9 | 22.7 | 23.0 |
| Zr | 272 | 264 | 255 | 223 | 218 | 358 | 367 | 364 | 274 | 365 | 275 | 371 | 351 | 306 | 217 | 234 | 251 |
| Nb | 78.1 | 76.9 | 74.9 | 65.6 | 62.0 | 107.9 | 98.8 | 98.2 | 72.0 | 98.6 | 73.1 | 100.6 | 106.0 | 79.9 | 57.2 | 68.6 | 61.5 |
| Cs | 1.78 | 0.57 | 0.49 | 0.44 | 0.39 | 0.62 | 0.65 | 0.65 | 0.51 | 0.62 | 0.49 | 0.61 | 0.65 | 0.46 | 0.40 | 0.42 | 0.32 |
| Ba | 550 | 536 | 528 | 508 | 454 | 654 | 614 | 613 | 482 | 612 | 482 | 613 | 654 | 473 | 465 | 479 | 552 |
| La | 45.3 | 43.1 | 43.7 | 37.7 | 35.0 | 70.9 | 49.9 | 50.1 | 35.7 | 49.7 | 36.1 | 50.1 | 70.0 | 38.4 | 28.9 | 36.8 | 42.9 |
| Ce | 89.2 | 84.0 | 84.9 | 73.9 | 69.3 | 133.2 | 96.4 | 95.9 | 70.8 | 96.5 | 70.8 | 97.1 | 132.8 | 75.4 | 57.4 | 72.4 | 89.2 |
| Pr | 10.77 | 10.35 | 10.22 | 8.98 | 8.51 | 16.14 | 11.60 | 11.56 | 8.73 | 11.67 | 8.59 | 11.82 | 16.09 | 9.10 | 7.03 | 8.86 | 10.81 |
| Nd | 42.0 | 40.6 | 40.4 | 35.5 | 33.6 | 61.9 | 45.1 | 44.4 | 34.2 | 45.0 | 33.8 | 45.0 | 62.2 | 35.8 | 28.4 | 35.2 | 43.6 |
| Sm | 8.75 | 8.44 | 8.34 | 7.58 | 7.09 | 12.13 | 9.18 | 9.09 | 7.19 | 9.13 | 7.20 | 9.16 | 12.16 | 7.49 | 6.22 | 7.28 | 8.83 |
| Eu | 2.90 | 2.79 | 2.78 | 2.51 | 2.43 | 4.01 | 3.04 | 3.03 | 2.50 | 3.07 | 2.50 | 3.09 | 4.04 | 2.59 | 2.16 | 2.47 | 2.76 |
| Gd | 7.29 | 6.91 | 6.98 | 6.60 | 6.11 | 9.80 | 7.57 | 7.42 | 6.41 | 7.60 | 6.30 | 7.51 | 9.86 | 6.56 | 5.74 | 6.54 | 8.02 |
| Tb | 1.00 | 0.99 | 1.00 | 0.92 | 0.89 | 1.30 | 1.01 | 0.98 | 0.89 | 1.01 | 0.90 | 1.00 | 1.31 | 0.91 | 0.81 | 0.93 | 1.11 |
| Dy | 4.95 | 4.93 | 4.86 | 4.85 | 4.68 | 5.93 | 4.56 | 4.58 | 4.38 | 4.58 | 4.41 | 4.61 | 5.90 | 4.50 | 4.20 | 4.72 | 5.08 |
| Ho | 0.86 | 0.83 | 0.85 | 0.87 | 0.82 | 0.92 | 0.70 | 0.70 | 0.75 | 0.70 | 0.76 | 0.70 | 0.92 | 0.75 | 0.76 | 0.84 | 0.86 |
| Er | 1.93 | 1.90 | 2.07 | 2.06 | 1.93 | 2.02 | 1.48 | 1.48 | 1.69 | 1.45 | 1.78 | 1.46 | 1.97 | 1.76 | 1.75 | 2.10 | 1.96 |
| Tm | 0.23 | 0.24 | 0.24 | 0.26 | 0.24 | 0.21 | 0.15 | 0.15 | 0.20 | 0.16 | 0.22 | 0.15 | 0.20 | 0.21 | 0.22 | 0.26 | 0.24 |
| Yb | 1.31 | 1.33 | 1.41 | 1.50 | 1.45 | 1.06 | 0.78 | 0.80 | 1.17 | 0.78 | 1.25 | 0.79 | 1.09 | 1.21 | 1.24 | 1.42 | 1.31 |
| Lu | 0.17 | 0.17 | 0.19 | 0.20 | 0.20 | 0.14 | 0.10 | 0.10 | 0.16 | 0.09 | 0.17 | 0.09 | 0.13 | 0.16 | 0.17 | 0.20 | 0.18 |
| Hf | 5.77 | 5.82 | 5.44 | 4.66 | 4.79 | 7.46 | 7.84 | 7.71 | 5.85 | 7.63 | 5.83 | 7.86 | 7.17 | 6.13 | 4.71 | 5.00 | 5.73 |
| Ta | 4.11 | 4.04 | 3.85 | 3.36 | 3.30 | 5.64 | 5.48 | 5.33 | 3.94 | 5.43 | 3.89 | 5.46 | 5.47 | 4.18 | 3.04 | 3.54 | 3.77 |
| Pb | 4.20 | 4.89 | 3.93 | 3.76 | 3.29 | 5.14 | 4.98 | 6.09 | 3.60 | 4.67 | 3.71 | 4.52 | 5.22 | 4.97 | 4.17 | 3.41 | 2.47 |
| Th | 5.49 | 5.39 | 5.13 | 4.31 | 4.09 | 7.95 | 7.00 | 6.93 | 4.84 | 6.93 | 4.94 | 6.91 | 7.70 | 5.34 | 3.63 | 4.41 | 4.15 |
| U | 1.38 | 1.36 | 1.27 | 1.08 | 1.06 | 1.77 | 1.82 | 1.93 | 1.28 | 1.84 | 1.31 | 1.82 | 1.76 | 1.40 | 0.95 | 1.12 | 1.04 |
| $(La/Yb)_N$ | 24.9 | 23.2 | 22.3 | 18.0 | 17.3 | 48.0 | 45.7 | 45.2 | 21.9 | 46.0 | 20.8 | 45.6 | 46.0 | 22.8 | 16.7 | 18.6 | 23.5 |
| $(Sm/Yb)_N$ | 7.4 | 7.0 | 6.6 | 5.6 | 5.4 | 12.7 | 13.0 | 12.7 | 6.8 | 13.1 | 6.4 | 12.9 | 12.4 | 6.9 | 5.6 | 5.7 | 7.5 |

*(continued on next page)*

**Table 2** (*continued*)

| Rock | Alkali basalts | | | | | | | | | | | | | | | | |
|---|---|---|---|---|---|---|---|---|---|---|---|---|---|---|---|---|---|
| Sample | D-13 | D-14 | D-15 | D-16 | D-17 | Z-1 | Z-2 | Z-3 | Z-4 | Z-5 | Z-6 | Z-7 | Z-8 | Z-9 | Z-10 | Z-11 | Z-12 |
| $(La/Sm)_N$ | 5.2 | 5.1 | 5.2 | 5.0 | 4.9 | 5.8 | 5.4 | 5.5 | 5.0 | 5.4 | 5.0 | 5.5 | 5.8 | 5.1 | 4.6 | 5.1 | 4.9 |
| Nb/Ta | 19.0 | 19.0 | 19.4 | 19.5 | 18.8 | 19.1 | 18.0 | 18.4 | 18.3 | 18.2 | 18.8 | 18.4 | 19.4 | 19.1 | 18.8 | 19.4 | 16.3 |
| Zr/Hf | 47.2 | 45.3 | 46.9 | 47.8 | 45.4 | 48.0 | 46.8 | 47.2 | 46.8 | 47.9 | 47.2 | 47.3 | 48.9 | 49.9 | 46.1 | 46.8 | 43.9 |
| Nb/Nb* | 1.71 | 1.74 | 1.73 | 1.78 | 1.79 | 1.57 | 1.82 | 1.82 | 1.89 | 1.83 | 1.89 | 1.86 | 1.57 | 1.92 | 1.93 | 1.86 | 1.59 |
| Ti/Ti* | 0.80 | 0.84 | 0.82 | 0.86 | 0.91 | 0.66 | 0.79 | 0.83 | 0.97 | 0.80 | 0.90 | 0.82 | 0.68 | 0.90 | 1.13 | 0.98 | 0.85 |
| Hf/Hf* | 0.76 | 0.79 | 0.75 | 0.72 | 0.78 | 0.68 | 0.97 | 0.97 | 0.94 | 0.95 | 0.94 | 0.97 | 0.66 | 0.94 | 0.89 | 0.79 | 0.73 |
| Eu/Eu* | 1.11 | 1.11 | 1.11 | 1.08 | 1.13 | 1.12 | 1.11 | 1.13 | 1.12 | 1.13 | 1.13 | 1.14 | 1.13 | 1.13 | 1.10 | 1.09 | 1.00 |

Trace elements in parts per million (ppm). $Eu/Eu^* = Eu_N / (Sm_N \times Gd_N)^{1/2}$, $Nb/Nb^* = Nb_N(Th_N \times La_N)^{1/2}$, $Hf/Hf^* = Hf_N / (Sm_N \times Nd_N)^{1/2}$, $Ti/Ti^* = Ti_N / (Nd_N^{-0.055} \times Sm_N^{0.333} \times Gd_N^{0.722})$ (Chen et al., 2009; Zeng et al., 2010), where subscript N denotes chondrite normalization (Sun and McDonough, 1989).

(Table 2). Some tholeiitic basalts display positive Pb anomalies, whereas others have negative anomalies (Fig. 4).

### 4.2. Melt inclusions

Primarily, well-preserved and randomly distributed melt inclusions with no visible cracks and no aureoles of secondary inclusions were selected for analysis in this study. The homogenization temperature of 1250 °C for inclusions is too high for olivine with low Fo. For these olivines, the melt inclusions were slightly overheated and required correction to be applied to their composition (e.g. Sobolev and Chaussidon, 1996). In addition, so-called "Fe-loss" resulting from post-entrapment re-equilibration with the host olivine has been observed within olivine-hosted melt inclusions (Danyushevsky et al., 2000). Previous studies have shown that the effects of overheating and underheating and possible associated Fe-loss by diffusion can be corrected using a computer application (FeO_Eq2.exe; Danyushevsky et al., 2000). Thus, the measured composition of these melt inclusions was corrected following a widely accepted procedure of Danyushevsky et al. (2000) and recalculated to be in equilibrium with the host olivine under the QFM buffer by applying another previously published model (Ford et al., 1983) using PROGRAM FeO_Eq2 V.3.2 software (Danyushevsky, 2000). This calculation requires an independent estimation of the total FeO content of the initial trapped melt, generally obtained from the total FeO variation trend of the whole rocks (Danyushevsky et al., 2000). Considering the total FeO content of alkali basalts is approximately constant and that there is a very small range of total FeO content (10.2–11.3%) for tholeiites (Table 1), we take their respective mean values as the respective total FeO content of the initial trapped alkali and tholeiitic basalt inclusions. The initial total FeO content of alkali and tholeiitic basalt inclusions are estimated to be 13 wt.% and 11 wt.%, respectively. The composition of original, uncorrected melt inclusions and corrected melt inclusion compositions together with the calculated Fe–Mg olivine–melt partition coefficients $K_D$, are given in Table S3 and Table S1, respectively. The calculated $K_D$ is consistent with well constrained experimental results ($0.30 \pm 0.03$) (Roeder and Emslie, 1970; Ulmer, 1989, Table S1).

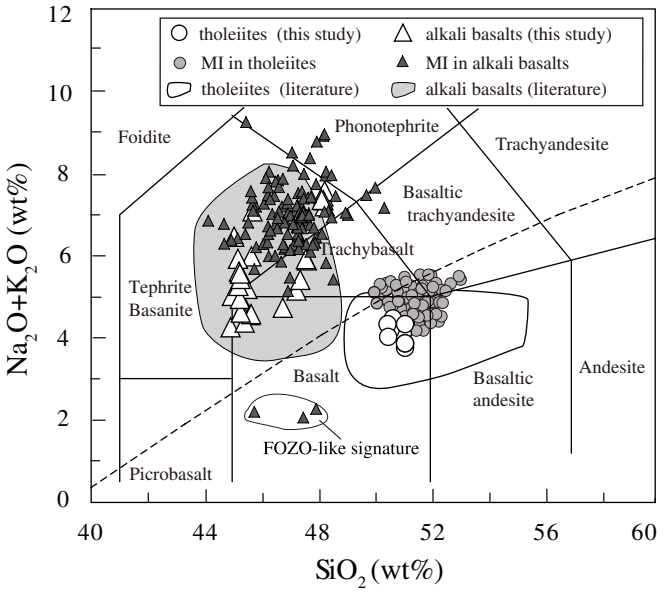


**Fig. 2.** Variation in total alkalis vs. $SiO_2$ for whole rocks and corrected melt inclusion compositions in olivine from the Hannuoba area (Le Bas et al., 1986). The line separating alkali basalts and tholeiites is from Macdonald and Katsura (1964). Large symbols represent the whole rock data and small symbols represent the melt inclusions. Open and gray shaded field denote the composition of the tholeiites and alkali basalts from Hannuoba, respectively (Zhi et al., 1990; Basu et al., 1991). Notably, three melt inclusions in alkali basalts with FOZO-like Pb isotopic compositions plot in the tholeiite field. Major element contents are normalized to 100% on a volatile-free basis. WR, whole rock; MI, melt inclusion.

On a total alkali–silica diagram (Fig. 2), the composition of melt inclusions from alkali basalts mostly plot in the basanite field, with some in the trachybasalt and basalt fields, and a few in the phonotephrite and basaltic trachyandesite fields. More specifically, three melt inclusions in the alkali basalts plot in the tholeiite field (Fig. 2). Most melt inclusions from tholeiitic basalts have compositions similar to those of their host rocks, plotting mainly near the intersection of the fields for basalt, trachybasalt, basaltic andesite and basaltic trachyandesite. MgO contents of melt inclusions from the tholeiitic and alkali basalts are 4–8 wt.% and 3.7–11.6 wt.%, respectively (Table S1). Melt inclusions in alkali basalts have higher $TiO_2$, and $K_2O$ but lower $SiO_2$ contents than melt inclusions in tholeiitic basalts at a given MgO content (Fig. 3). The $CaO/Al_2O_3$ ratios within a single series (tholeiitic or alkalic series) display significantly different evolutionary trends (Fig. 3). The melt inclusions in tholeiitic basalts exhibit a limited range of major element composition, in contrast to the relatively wide range for melt inclusions in alkali basalts (Fig. 3). In addition, there is considerable scatter of other major element compositions at a given MgO content compared with whole rock compositions (Fig. 3). In general, variations of chemical compositions of melt inclusions are consistent with compositional trends defined by the whole rock compositions.

Lead isotope data of 140 melt inclusions in olivine from the alkali and tholeiitic basalts are reported in Table 3 and Fig. 5. $^{208}Pb/^{206}Pb$ and $^{207}Pb/^{206}Pb$ of melt inclusions vary from 2.0718 to 2.195 and from 0.8278 to 0.912, respectively (Table 3). The lead isotopic composition of melt inclusions in the alkali basalts is similar to those of the whole rocks, except for three melt inclusions that have low $^{207}Pb/^{206}Pb$ and $^{208}Pb/^{206}Pb$ (Fig. 5). With the exception of these three samples, melt inclusions in the alkali basalts display very limited Pb isotopic variation. In contrast, Pb isotopic compositions of melt inclusions in the tholeiites vary significantly and extend toward an EM1-type isotopic composition (Fig. 5).

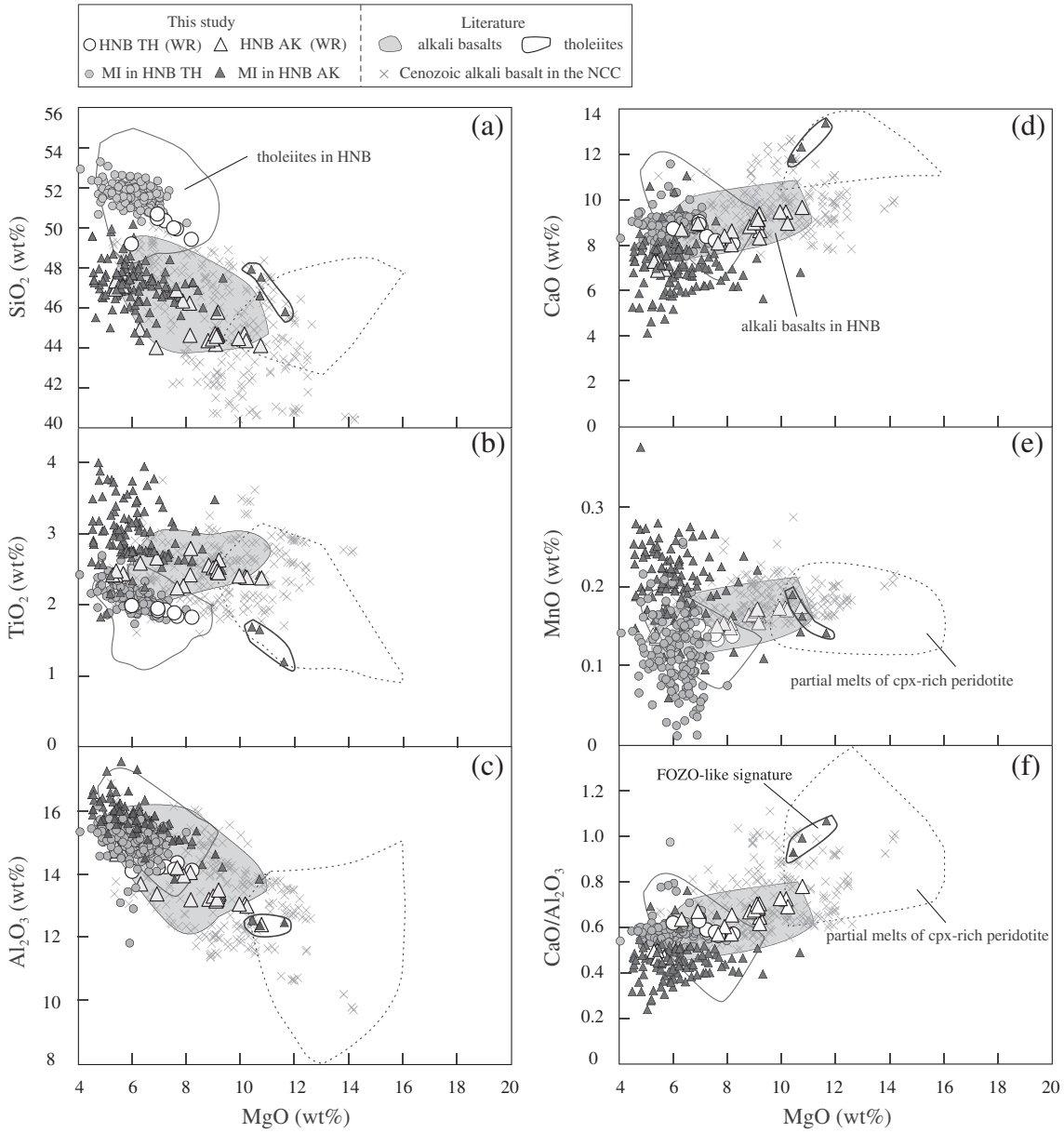


**Fig. 3.** (a)–(f) Variation of $SiO_2$, $TiO_2$, $Al_2O_3$, CaO, MnO and $CaO/Al_2O_3$ vs MgO for bulk rocks and melt inclusions in Hannuoba basalts, after correction. Major element contents are normalized to 100% on a volatile-free basis. The gray crosses represent the data from other Cenozoic alkali basalts in the NCC. Clinopyroxene (cpx)-rich peridotite: mixture of clinopyroxenite and peridotite (Sorbadere et al., 2013); wehrlites (Médard et al., 2006). Whole-rock major-element compositions of Cenozoic alkali basalts in the NCC are those of previous studies (Xu et al., 2005, 2012a; Tang et al., 2006; Choi et al., 2008; Ho et al., 2008; Liu et al., 2008; Chen et al., 2009; Zhang et al., 2009; Zeng et al., 2010, 2011; Wang et al., 2011; Xu et al., 2012b; Zhang et al., 2012; Sakuyama et al., 2013). Symbols for bulk rocks and melt inclusions in Hannuoba basalts are the same as in Fig. 2.

### 4.3. Olivine compositions

The composition of olivines from alkali and tholeiitic basalts is listed in Table S2. The olivine has a relatively wide range of Fo content varying from 68 to 87.3. In general, olivine crystals present in thin sections have euhedral to subhedral shapes. CaO (>0.10 wt.%) contents of most of the olivine crystals in both the tholeiitic and alkali basalts are generally higher than those of olivines in mantle xenoliths (CaO < 0.1 wt.%) (Thompson and Gibson, 2000; Ren et al., 2004; Rudnick et al., 2004; Tang et al., 2007; Fig. 6a). The NiO content of olivine is similar to those of Hawaiian olivine but higher than those of the "common olivine" field (olivine in mantle xenoliths, oceanic abyssal peridotites and MORBs, orogenic massifs and ophiolites) defined by Sobolev et al. (2005) for a given Fo value. NiO shows a positive correlation with Fo content that differs from the mantle olivine array (Sato, 1977; Fig. 6b). All of these characteristics suggest that most of the olivine crystals in these basalts are likely to be magmatic in origin. Consistent with the characteristics of whole rock major element compositions, the olivine crystals in the tholeiites display a limited range of compositional variation, while those from the alkali basalts display a much wider range.

## 5. Discussion

### 5.1. Crustal contamination

Many previous studies have suggested that the effect of crustal contamination on the composition of Cenozoic Hannuoba basalts appears to be insignificant (Song et al., 1990; Zhi et al., 1990; Basu et al., 1991; Choi et al., 2008). Additionally, the presence of mantle-derived xenoliths in the Hannuoba alkali basalts implies that the host

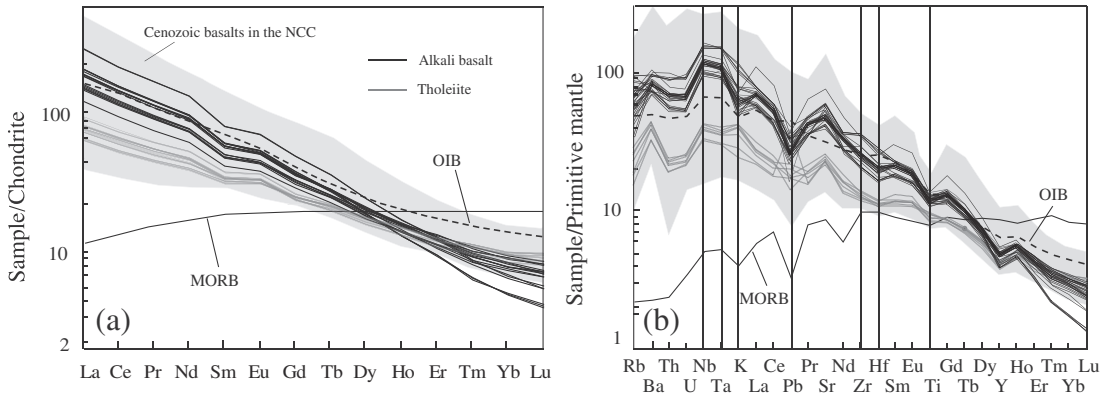


**Fig. 4.** Spidergrams of trace element distributions for Hannuoba basalts, NCC. (a) Chondrite-normalized REE patterns for alkali and tholeiitic basalts; the chondrite REE composition is after Sun and McDonough (1989). (b) Primitive mantle-normalized trace element patterns for alkali and tholeiitic basalts; the primitive mantle composition is after McDonough and Sun (1995). N-MORB and OIB data are from Sun and McDonough (1989). Whole-rock trace-element compositions of Cenozoic basalts from the NCC are from previous studies (Zhi et al., 1990; Basu et al., 1991; Xu et al., 2005, 2012a; Tang et al., 2006; Choi et al., 2008; Ho et al., 2008; Liu et al., 2008; Chen et al., 2009; Zhang et al., 2009; Zeng et al., 2010, 2011; Wang et al., 2011; Hong et al., 2013; Xu et al., 2012b; Zhang et al., 2012; Sakuyama et al., 2013).

lavas would have ascended rapidly toward the surface and therefore were not significantly affected by crustal contamination. Strong positive anomalies of Nb and Ta in the trace elements patterns of the Hannuoba basalts also argue against significant crustal contamination. The low Ce/Pb of the Hannuoba tholeiites could potentially be explained by contamination of continental crust. However, Nb/U ratios (48.2–61.5) of the Hannuoba tholeiites and alkali basalts (Fig. 7a) are higher than those of average OIB and MORB and are much greater than those of average continental crust (Nb/U ≈ 10) (Hofmann et al., 1986).

### 5.2. Possible petrogenetic processes and the nature of the mantle source of the Cenozoic basalts

Melt inclusions in the alkali and tholeiitic basalts lie on the compositional trends defined by the corresponding bulk rock compositions (Fig. 3). CaO contents and $CaO/Al_2O_3$ ratios of the alkali suite (including alkali basalts and melt inclusions in alkali basalts) show positive correlations with MgO contents (Fig. 3). These characteristics could be ascribed to fractional crystallization of clinopyroxene in the magmatic plumbing system. However, this can be ruled out for several reasons. As previously argued, the presence of mantle-derived xenoliths in the Hannuoba basalts implies that the host lavas ascended rapidly, without having time to experience significant fractional crystallization. As shown in Fig. 6, the compositional variation of olivine in the alkali basalts also argues against fractional crystallization of clinopyroxene. The negative correlation of Sm/Yb with $CaO/Al_2O_3$ in the alkali basalts also does not support fractional crystallization of clinopyroxene, which cannot result in substantial fractionation Sm from Yb (Fig. 8b). Moreover, the large variation of incompatible trace element ratios, such as Ce/Pb and Ba/Th in the alkali basalts (Fig. 7b, d) cannot be explained by fractional crystallization. On the other hand, the negative correlation of La/Yb with MgO content in the alkali basalts is largely consistent with mixing of melts of pyroxenite and peridotite (Fig. 8a). The $(Gd/Yb)_n$ ratios of the alkali basalts are high (3.47–8.06) (Table 2), reflecting the presence of residual garnet in the source during melting (Kamenetsky et al., 2012). Hence, the compositional characteristics of the alkali basalts are largely controlled by magma mixing and partial melting. The limited fractional crystallization of olivine cannot, however, be completely precluded and the process of fractional crystallization may be involved in the formation of alkali basalts with very low MgO contents (Fig. 8a).

Partial melting modeling indicates that the major and trace element compositions of alkali basalts can be produced by melting garnet pyroxenite and peridotite (Fig. 8a, d). As shown in Fig. 8, alkali basalts with relatively low MgO content and high La/Yb and Zr/Hf could be generated from partial melting of the dominant garnet–pyroxenite. The alkali basalts with high MgO content and low La/Yb and Zr/Hf are consistent with a greater garnet peridotite component in the mantle source (Fig. 8a, d). In addition, the high Zn/Fe, Fe/Mn and low Co/Fe ratios of the alkali basalts (Fig. 9) may also indicate the presence of garnet–pyroxenite in the source as experimental studies have shown that compared to melts of peridotite, partial melts of pyroxenite would have high Zn/Fe, Fe/Mn and low Co/Fe (Le Roux et al., 2011).

As discussed above, the Pb isotopic composition of the three melt inclusions (D 3-1, D-8(3)-3, D-17(2)-5) in the alkali basalts with low $^{207}Pb/^{206}Pb$ and $^{208}Pb/^{206}Pb$ differs from those of whole rocks and plot very close to the FOZO field (Hart et al., 1992) (Fig. 5). These melt inclusions have relatively high CaO and $CaO/Al_2O_3$ levels (Fig. 3d, f). In fact, Cenozoic basalts with high $CaO/Al_2O_3$ ratios and MgO contents extending to 1.1 and 14.2, respectively, have been recently reported from the eastern NCC (Fig. 3, Sakuyama et al., 2013). As shown in Fig. 3, melt inclusions with high CaO and $CaO/Al_2O_3$ content may be derived from partial melting of clinopyroxene-rich peridotite.

The constant La/Yb at variable MgO content in tholeiites from Hannuoba can be attributed to crystal fractionation (Fig. 8a). However, a wide range of isotopic composition of the tholeiitic suite largely reflects a characteristic of the source region (Figs. 5, 8c). Partial melt modeling indicates that tholeiites with low La/Yb and Zr/Hf are consistent with a greater proportion of garnet peridotite in their source relative to that of the alkali basalts (Fig. Fig. 8a, 8d).

### 5.3. Origin of the alkali basalt suite

As discussed above, low MgO alkali basalts with low CaO, and $CaO/Al_2O_3$ are derived from small degrees of partial melting of garnet–pyroxenite. Experimental results suggest that partial melts of silica under-saturated garnet pyroxenite are similar to alkali basalts in composition (Hirschmann et al., 2003). Pyroxenite of metasomatic origin in the lithosphere is likely to be the source rock considering the strong enrichment in incompatible trace elements within the alkali basalts. In addition, the alkali basalts from Hannuoba show a characteristic depletion in K and Ti in primitive mantle normalized trace element diagrams (Fig. 4). This feature is commonly attributed to the presence of amphibole and/or phlogopite as residual minerals during partial melting (Class and Goldstein, 1997; Le Roex et al., 2001). As amphibole and phlogopite are unstable in the asthenospheric mantle and only stable in the subcontinental lithosphere, this indicates the involvement of a lithospheric mantle component in the mantle source (Class and Goldstein, 1997). Another prominent compositional feature of the alkali basalts is the negative correlation between Ba/Th and Sm/Yb, implying

**Table 3**
Pb isotopic compositions of melt inclusions from Hannuoba basalts.

| Melt inclusions in tholeiites | | | | | | | | | |
|---|---|---|---|---|---|---|---|---|---|
| Sample | $^{208}Pb/^{206}Pb$ | Stderr | $^{207}Pb/^{206}Pb$ | Stderr | Sample | $^{208}Pb/^{206}Pb$ | Stderr | $^{207}Pb/^{206}Pb$ | Stderr |
| D-10(2)-1 | 2.1502 | 0.0014 | 0.8846 | 0.0006 | D-10(8)-3 | 2.1712 | 0.0024 | 0.8908 | 0.0010 |
| D-10(2)-2 | 2.1817 | 0.0027 | 0.9000 | 0.0015 | D-20(1)-1 | 2.1752 | 0.0019 | 0.8974 | 0.0009 |
| D-10(2)-3 | 2.1705 | 0.0019 | 0.8921 | 0.0008 | D-20(1)-2 | 2.1756 | 0.0016 | 0.8979 | 0.0008 |
| D-10(2)-4 | 2.1722 | 0.0013 | 0.8982 | 0.0007 | D-20(1)-3 | 2.1517 | 0.0020 | 0.8861 | 0.0011 |
| D-10(2)-5 | 2.1528 | 0.0016 | 0.8836 | 0.0008 | D-20(1)-4 | 2.1484 | 0.0024 | 0.8835 | 0.0010 |
| D-10(2)-6 | 2.1616 | 0.0033 | 0.8834 | 0.0016 | D-20(1)-5 | 2.1732 | 0.0016 | 0.8976 | 0.0007 |
| D-10(2)-7 | 2.1737 | 0.0042 | 0.8995 | 0.0022 | D-20(1)-7 | 2.1759 | 0.0015 | 0.8959 | 0.0009 |
| D-10(3)-1 | 2.1732 | 0.0022 | 0.8986 | 0.0011 | D-20(4)-1 | 2.1742 | 0.0023 | 0.8979 | 0.0017 |
| D-10(3)-2 | 2.1733 | 0.0015 | 0.8974 | 0.0008 | D-20(4)-4 | 2.1799 | 0.0019 | 0.8990 | 0.0010 |
| D-10(3)-4 | 2.1670 | 0.0034 | 0.8919 | 0.0017 | D-20(4)-5 | 2.1726 | 0.0013 | 0.8960 | 0.0007 |
| D-10(3)-5 | 2.1758 | 0.0017 | 0.8995 | 0.0010 | D-20(4)-6 | 2.1664 | 0.0016 | 0.8953 | 0.0007 |
| D-10(3)-6 | 2.1709 | 0.0030 | 0.8946 | 0.0017 | D-20(4)-7 | 2.1728 | 0.0030 | 0.8915 | 0.0017 |
| D-10(5)-1 | 2.1770 | 0.0023 | 0.9019 | 0.0013 | D-20(5)-1 | 2.1712 | 0.0028 | 0.8957 | 0.0012 |
| D-10(5)-2 | 2.1687 | 0.0069 | 0.8886 | 0.0031 | D-20(5)-3 | 2.1730 | 0.0023 | 0.8965 | 0.0011 |
| D-10(5)-3 | 2.1683 | 0.0016 | 0.8962 | 0.0009 | D-20(5)-4 | 2.1774 | 0.0021 | 0.8971 | 0.0011 |
| D-10(5)-4 | 2.1796 | 0.0017 | 0.8990 | 0.0008 | D-20(5)-5 | 2.1936 | 0.0013 | 0.9073 | 0.0007 |
| D-10(5)-6 | 2.1772 | 0.0015 | 0.8996 | 0.0006 | D-20(5)-6 | 2.1793 | 0.0014 | 0.8961 | 0.0007 |
| D-10(5)-8 | 2.1790 | 0.0019 | 0.8983 | 0.0010 | D-20(6)-2 | 2.1744 | 0.0021 | 0.8945 | 0.0011 |
| D-10(6)-1 | 2.1650 | 0.0014 | 0.8917 | 0.0008 | D-20(6)-4 | 2.1947 | 0.0013 | 0.9118 | 0.0007 |
| D-10(6)-2 | 2.1763 | 0.0022 | 0.8969 | 0.0010 | D-20(6)-5 | 2.1827 | 0.0030 | 0.8995 | 0.0014 |
| D-10(6)-3 | 2.1767 | 0.0038 | 0.8951 | 0.0020 | D-20(6)-6 | 2.1783 | 0.0017 | 0.8984 | 0.0008 |
| D-10(6)-4 | 2.1767 | 0.0020 | 0.8971 | 0.0009 | D-20(6)-7 | 2.1744 | 0.0020 | 0.8955 | 0.0009 |
| D-10(6)-5 | 2.1514 | 0.0021 | 0.8832 | 0.0010 | D-20(8)-1 | 2.1701 | 0.0019 | 0.8955 | 0.0009 |
| D-10(6)-6 | 2.1799 | 0.0014 | 0.9011 | 0.0007 | D-20(8)-3 | 2.1771 | 0.0014 | 0.8992 | 0.0007 |
| D-10(6)-7 | 2.1305 | 0.0035 | 0.8746 | 0.0017 | D-20(8)-5 | 2.1767 | 0.0019 | 0.8977 | 0.0008 |
| D-10(7)-1 | 2.1729 | 0.0014 | 0.8966 | 0.0007 | D-20(8)-6 | 2.1765 | 0.0014 | 0.8992 | 0.0007 |
| D-10(7)-2 | 2.1667 | 0.0031 | 0.8922 | 0.0017 | D-20(9)-2 | 2.1804 | 0.0015 | 0.9007 | 0.0007 |
| D-10(7)-4 | 2.1720 | 0.0054 | 0.8952 | 0.0028 | D-20(9)-3 | 2.1830 | 0.0043 | 0.9008 | 0.0020 |
| D-10(7)-5 | 2.1761 | 0.0015 | 0.8974 | 0.0007 | D-20(9)-4 | 2.1821 | 0.0015 | 0.9010 | 0.0008 |
| D-10(7)-6 | 2.1594 | 0.0022 | 0.8904 | 0.0010 | D-20(9)-5 | 2.1626 | 0.0037 | 0.8874 | 0.0018 |
| D-10(7)-7 | 2.1707 | 0.0016 | 0.8964 | 0.0008 | D-20(9)-6 | 2.1804 | 0.0019 | 0.8970 | 0.0011 |
| D-10(8)-1 | 2.1773 | 0.0025 | 0.9002 | 0.0012 | D-20(9)-7 | 2.1571 | 0.0014 | 0.8869 | 0.0008 |
| D-10(8)-2 | 2.1735 | 0.0028 | 0.8950 | 0.0017 | | | | | |
| *Melt inclusions in alkali basalts* | | | | | | | | | |
| D-3-1 | ***2.0718*** | ***0.0017*** | ***0.8278*** | ***0.0009*** | D-8(8)-2 | 2.1315 | 0.0020 | 0.8724 | 0.0010 |
| D-3-2 | 2.1319 | 0.0029 | 0.8675 | 0.0016 | D-8(8)-3 | 2.1353 | 0.0037 | 0.8724 | 0.0016 |
| D-3-3 | 2.1294 | 0.0021 | 0.8720 | 0.0012 | D-8(8)-4 | 2.1333 | 0.0017 | 0.8719 | 0.0008 |
| D-3-4 | 2.1352 | 0.0023 | 0.8739 | 0.0012 | D-8(8)-5 | 2.1395 | 0.0023 | 0.8730 | 0.0011 |
| D-3-5 | 2.1299 | 0.0016 | 0.8727 | 0.0009 | D-8(8)-7 | 2.1376 | 0.0023 | 0.8724 | 0.0011 |
| D-3-6 | 2.1346 | 0.0022 | 0.8736 | 0.0011 | D-8(9)-1 | 2.1366 | 0.0027 | 0.8715 | 0.0010 |
| D-8(1)-1 | 2.1380 | 0.0016 | 0.8737 | 0.0008 | D-8(9)-2 | 2.1404 | 0.0153 | 0.8756 | 0.0072 |
| D-8(1)-3 | 2.1481 | 0.0038 | 0.8739 | 0.0018 | D-8(9)-3 | 2.1367 | 0.0014 | 0.8724 | 0.0008 |
| D-8(1)-4 | 2.1378 | 0.0036 | 0.8755 | 0.0020 | D-8(9)-4 | 2.1368 | 0.0020 | 0.8724 | 0.0010 |
| D-8(3)-2 | 2.1346 | 0.0029 | 0.8761 | 0.0010 | D-8(9)-5 | 2.1398 | 0.0017 | 0.8744 | 0.0009 |
| D-8(3)-3 | ***2.0889*** | ***0.0201*** | ***0.8410*** | ***0.0098*** | D-8(9)-7 | 2.1494 | 0.0041 | 0.8753 | 0.0023 |
| D-8(3)-5 | 2.1349 | 0.0046 | 0.8678 | 0.0019 | D-16(4)-1 | 2.1398 | 0.0018 | 0.8728 | 0.0008 |
| D-8(3)-6 | 2.1511 | 0.0138 | 0.8829 | 0.0072 | D-16(4)-2 | 2.1348 | 0.0023 | 0.8730 | 0.0011 |
| D-8(3)-7 | 2.1372 | 0.0027 | 0.8724 | 0.0011 | D-16(4)-3 | 2.1423 | 0.0033 | 0.8701 | 0.0018 |
| D-8(3)-8 | 2.1307 | 0.0038 | 0.8680 | 0.0017 | D-16(4)-4 | 2.1381 | 0.0018 | 0.8746 | 0.0011 |
| D-8(4)-1 | 2.1404 | 0.0028 | 0.8697 | 0.0013 | D-16(4)-5 | 2.1421 | 0.0024 | 0.8727 | 0.0012 |
| D-8(4)-2 | 2.1465 | 0.0090 | 0.8717 | 0.0038 | D-16(4)-6 | 2.1476 | 0.0037 | 0.8753 | 0.0017 |
| D-8(4)-3 | 2.1312 | 0.0034 | 0.8704 | 0.0014 | D-16(4)-7 | 2.1365 | 0.0023 | 0.8712 | 0.0011 |
| D-8(4)-4 | 2.1362 | 0.0040 | 0.8717 | 0.0020 | D-16(5)-1 | 2.1381 | 0.0023 | 0.8729 | 0.0008 |
| D-8(4)-5 | 2.1384 | 0.0023 | 0.8748 | 0.0009 | D-16(5)-2 | 2.1403 | 0.0026 | 0.8730 | 0.0011 |
| D-8(4)-6 | 2.1327 | 0.0028 | 0.8687 | 0.0017 | D-16(5)-4 | 2.1426 | 0.0050 | 0.8731 | 0.0026 |
| D-8(5)-2 | 2.1433 | 0.0025 | 0.8716 | 0.0011 | D-16(5)-5 | 2.1438 | 0.0020 | 0.8736 | 0.0010 |
| D-8(5)-3 | 2.1312 | 0.0031 | 0.8754 | 0.0014 | D-16(5)-6 | 2.1399 | 0.0022 | 0.8732 | 0.0011 |
| D-8(5)-5 | 2.1334 | 0.0021 | 0.8712 | 0.0009 | D-16(5)-7 | 2.1437 | 0.0032 | 0.8732 | 0.0012 |
| D-8(5)-6 | 2.1285 | 0.0025 | 0.8680 | 0.0017 | D-16(6)-2 | 2.1430 | 0.0025 | 0.8778 | 0.0010 |
| D-8(5)-7 | 2.1355 | 0.0053 | 0.8735 | 0.0022 | D-16(6)-5 | 2.1423 | 0.0040 | 0.8763 | 0.0022 |
| D-8(6)-2 | 2.1349 | 0.0016 | 0.8721 | 0.0007 | D-17(1)-2 | 2.1377 | 0.0021 | 0.8708 | 0.0011 |
| D-8(6)-4 | 2.1302 | 0.0020 | 0.8702 | 0.0009 | D-17(1)-3 | 2.1373 | 0.0015 | 0.8721 | 0.0009 |
| D-8(6)-6 | 2.1363 | 0.0024 | 0.8750 | 0.0012 | D-17(1)-5 | 2.1355 | 0.0023 | 0.8719 | 0.0012 |
| D-8(6)-7 | 2.1366 | 0.0031 | 0.8753 | 0.0023 | D-17(1)-6 | 2.1357 | 0.0017 | 0.8719 | 0.0008 |
| D-8(7)-1 | 2.1339 | 0.0022 | 0.8723 | 0.0010 | D-17(1)-7 | 2.1350 | 0.0024 | 0.8730 | 0.0011 |
| D-8(7)-2 | 2.1349 | 0.0016 | 0.8721 | 0.0007 | D-17(2)-1 | 2.1326 | 0.0017 | 0.8706 | 0.0009 |
| D-8(7)-3 | 2.1348 | 0.0015 | 0.8723 | 0.0008 | D-17(2)-2 | 2.1298 | 0.0014 | 0.8696 | 0.0008 |
| D-8(7)-4 | 2.1302 | 0.0020 | 0.8702 | 0.0009 | D-17(2)-3 | 2.1338 | 0.0014 | 0.8731 | 0.0007 |
| D-8(7)-5 | 2.1441 | 0.0025 | 0.8749 | 0.0013 | D-17(2)-4 | 2.1389 | 0.0021 | 0.8730 | 0.0011 |
| D-8(7)-6 | 2.1363 | 0.0024 | 0.8750 | 0.0012 | D-17(2)-5 | ***2.0932*** | ***0.0048*** | ***0.8362*** | ***0.0020*** |
| D-8(7)-7 | 2.1417 | 0.0041 | 0.8737 | 0.0017 | Z-6(3)-4 | 2.1379 | 0.0023 | 0.8665 | 0.0049 |
| D-8(8)-1 | 2.1317 | 0.0022 | 0.8732 | 0.0009 | | | | | |

Melt inclusions (D-3-1, D-8(3)-3, D-17(2)-5, indicated in bold and italics) are outliers with Pb isotopic compositions similar to FOZO. Stderr, standard error.

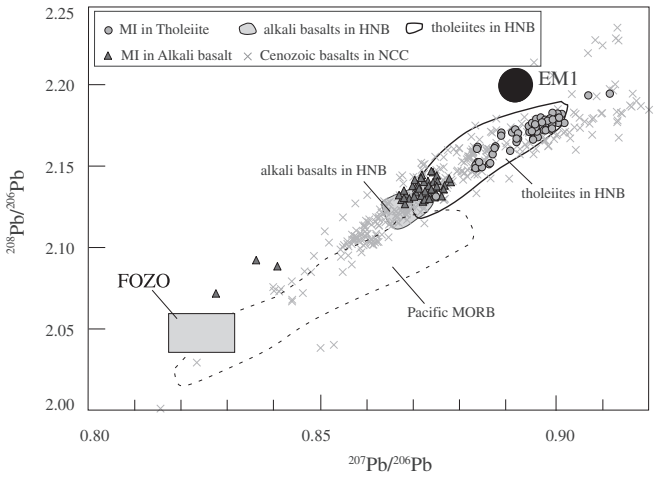


**Fig. 5.** $^{208}Pb/^{206}Pb$ and $^{207}Pb/^{206}Pb$ of melt inclusions from Hannuoba basalts. Open and gray shaded field denote the Pb isotopic compositions of the tholeiites and alkali basalts from Hannuoba, respectively (Song et al., 1990; Basu et al., 1991). Pb isotopic composition of the Pacific MORBs is based on data compiled by Stracke et al. (2003), and the composition of the EM1 end-member is modified after Saal et al. (2005). The gray crosses represent data from other Cenozoic basalts in the NCC (Basu et al., 1991; Xu et al., 2005, 2012a; Tang et al., 2006; Choi et al., 2008; Ho et al., 2008; Liu et al., 2008; Chen et al., 2009; Zhang et al., 2009; Zeng et al., 2011; Wang et al., 2011; Xu et al., 2012b; Zhang et al., 2012; Sakuyama et al., 2013).

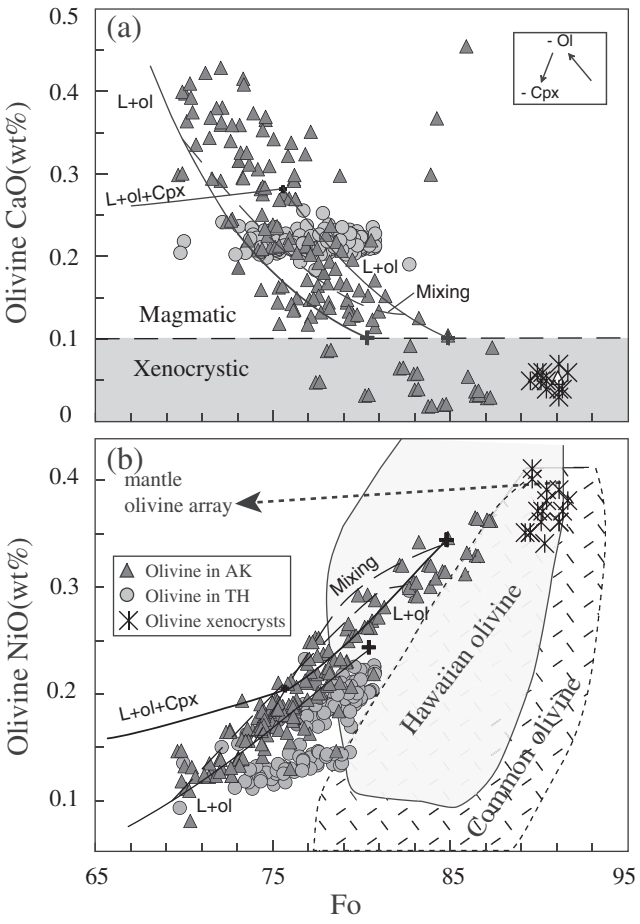


**Fig. 6.** Chemical variations of olivine in Hannuoba basalts. (a) Fo versus wt.% CaO. The dashed line that separates magmatic and xenocrystic olivine on the basis of CaO is after Thompson and Gibson (2000). (b) Fo versus wt.% NiO. The "common olivine" field is from Sobolev et al. (2005) based on olivine in mantle xenoliths, oceanic abyssal peridotites and mid-ocean-ridge basalts, orogenic massifs and ophiolites, while the Hawaiian olivine field outlines the range for olivine from Hawaiian basalts (Sobolev et al., 2005). The black lines are for olivine compositions that crystallize from two assumed magmas that subsequently fractionated olivine and clinopyroxene, and olivine, respectively (Herzberg et al., 2014). The dashed line is for olivine that crystallized from mixed magmas. The mantle olivine array is from Sato (1977). Olivine xenocrysts are from the literature (Rudnick et al., 2004; Tang et al., 2007), based on olivine in spinel peridotite from Hannuoba.

that a residual mineral phase fractionating Ba from Th was present during partial melting (Fig. 7d). This mineral phase could be phlogopite as phlogopite fractionates Ba from Th (LaTourrette et al., 1995; Foley et al., 1996). Additionally, the variation of Ce/Pb ratios observed for alkali basalt is consistent with partial melting of a source containing residual phlogopite, which is a potentially important reservoir for Pb in the mantle (Rosenbaum, 1993). Hence, the alkali basalts probably represent partial melts primarily originating from phlogopite-bearing metasomatic garnet pyroxenite in the lithospheric mantle. Amphibole and phlogopite, as the K-bearing constituents in the mantle, have been suggested to play a crucial role in the formation of alkaline magmas (Class and Goldstein, 1997; Niu and O'Hara, 2003; Pilet et al., 2008, 2011). Pyroxenite of metasomatic origin in the lithosphere may have formed recently, as evidenced by spinel peridotite xenoliths from Cenozoic Hannuoba basalts markedly different from typical cratonic lithosphere, implying the replacement of the Archean mantle lithosphere beneath the NCC (Rudnick et al., 2004).

As discussed above, the three melt inclusions in the alkali basalts with low $^{207}Pb/^{206}Pb$ and $^{208}Pb/^{206}Pb$ are isotopically distinct from the whole rocks and plot close to the FOZO field (Hart et al., 1992) (Fig. 5). The proportion of the source component with a FOZO-like composition must be quite small, since only three of the alkali basalt melt inclusions display this Pb isotopic signature (Fig. 5). The major element characteristics of these three inclusions (Fig. 3) suggest that this minor source component may be composed of cpx-rich peridotite.

### 5.4. Origin of the tholeiite suite

As shown in Fig. 5, Pb isotopic compositions of olivine-hosted melt inclusions in tholeiites vary significantly and extend toward EM1-type isotopic composition, indicating that a component with high $^{208}Pb/^{206}Pb$ and $^{207}Pb/^{206}Pb$ ratios was involved in the petrogenesis of the Hannuoba basalts. A young Pacific slab, as proposed by previous studies can be precluded as the source material for the EM1-like signature because of the relatively low $^{207}Pb/^{206}Pb$ ratio of Pacific MORB (Fig. 5). As argued by Thirlwall (1997), the formation of an EM1-like signature with high $^{207}Pb/^{206}Pb$ ratio requires the source material to be isolated for a long period of time (>1 Ga).

Recycled ancient oceanic crust and sediment isolated for >1 Ga are likely to be the source materials for the EM1-type Pb isotopic component. Oceanic and continental basalts with EM1-like characteristics have been often ascribed to the presence of recycled ancient oceanic crust and sediment in their mantle source (Hofmann, 1997; Rehkamper and Hofmann, 1997; Eisele et al., 2002; Murphy et al., 2002; Ren et al., 2006, 2009; Rapp et al., 2008). As illustrated in Fig. 9b, the Zn/Fe, Fe/Mn and Co/Fe ratios of the tholeiites, slightly higher than those of partial melts of peridotite, imply that a mixture of peridotite with small amounts of pyroxenite is present in the source. The formation of the pyroxenite component involved in the mantle source of the tholeiites may be related to recycled ancient oceanic crust and sediment. Given the relatively high $^{207}Pb/^{206}Pb$ and high $^{208}Pb/^{206}Pb$ isotopes of the ancient lower oceanic crust (Thirlwall, 1997), it may have been involved in the generation of EM1-type basalts. Additionally, the enrichment of Eu and Sr in the tholeiites (Fig. 4) is most likely inherited from a source region containing lower oceanic crust, as positive Eu anomalies are a typical characteristic of oceanic gabbro (Stracke et al., 2003). Experimental studies have also confirmed that positive Eu anomalies combined with silica-saturation of partial melts are indicative of a recycled gabbroic component in the mantle

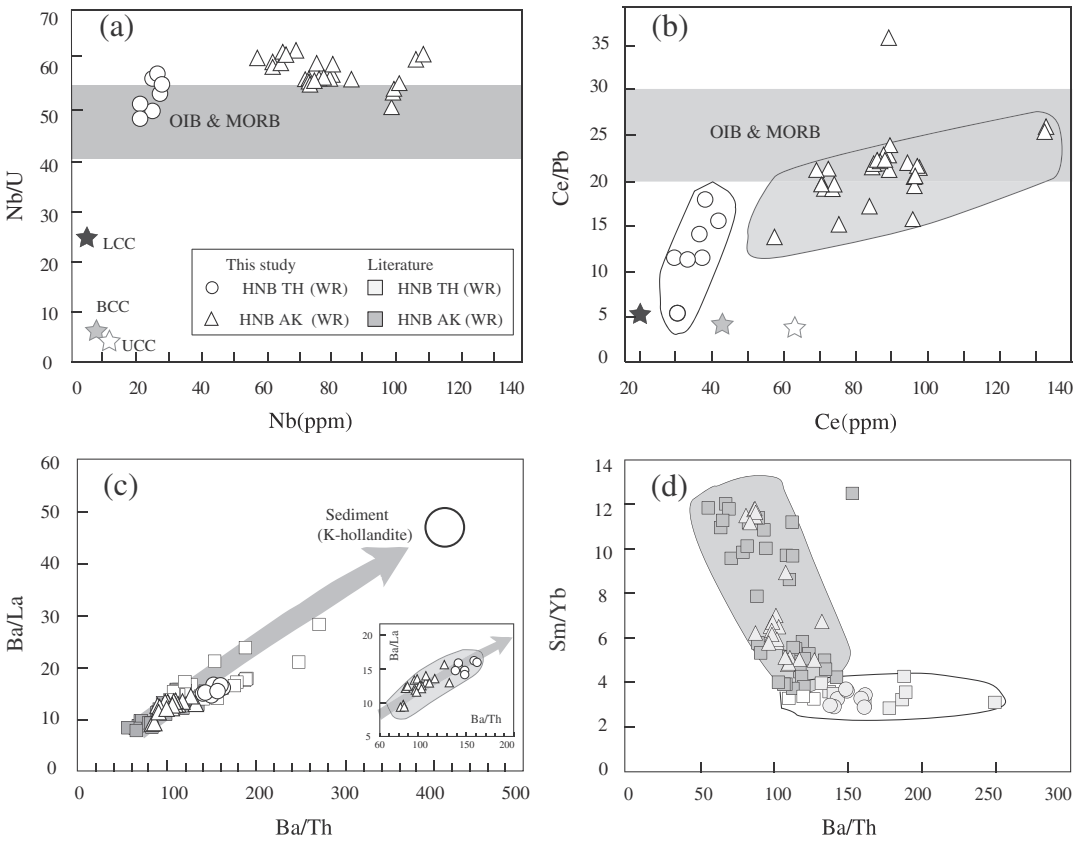


**Fig. 7.** (a) Nb/U versus Nb; (b) Ce/Pb versus Ce; (c) Ba/La versus Ba/Th, (d) Ba/Th versus Sm/Yb. Data for MORB and OIB are from Hofmann et al. (1986). Data for K-hollandite ($KAlSi_3O_8$) is from Rapp et al. (2008). Experimental studies have demonstrated that in subducted material, K-hollandite in sediments is the only major phase that can release significant amounts of incompatible elements such as Ba and Pb (Rapp et al., 2008). Also shown for reference are the compositions of upper continental crust (UCC), lower continental crust (LCC) and bulk continental crust (BCC) from Rudnick and Gao (2003). The white and gray squares are literature data for tholeiites and alkali basalts, respectively (Zhi et al., 1990; Basu et al., 1991). HNB AK indicates Hannuoba alkali basalts. HNB TH indicates Hannuoba tholeiites. The symbols for Hannuoba basalts are the same as in Fig. 2.

source of plume-related magmas (Kogiso et al., 2003; Yaxley & Sobolev, 2007). Hence, addition of a recycled oceanic gabbroic component to the mantle source can best account for the positive Sr and Eu anomalies and silica-saturation of the Hannuoba tholeiites. Because recycled gabbro has low $^{87}Sr/^{86}Sr$ and a very low Rb/Sr ratio (Stracke et al., 2003), small amounts of a recycled ancient sedimentary component is required to explain the more radiogenic Sr isotope composition of the tholeiites (Song et al., 1990; Basu et al., 1991). Experimental studies have recently demonstrated that trace element characteristics of OIB with an EM1-like isotopic signature can be partially ascribed to the involvement of recycled ancient K-hollandite-bearing sediments in the mantle source (Rapp et al., 2008). As illustrated in Fig. 7, K-hollandite plotting on the extension of the compositional trend defined by the Ba/La and Ba/Th ratios of the Hannuoba basalts suggests that small amounts of a sedimentary component was present in the mantle source of the Hannuoba basalts. The Hannuoba tholeiites have positive K anomalies, and some have positive Pb anomalies and low Ce/Pb ratios (Fig. 4b, 7b). These features are also consistent with the presence of gabbro and sedimentary components in the mantle source. Therefore, the source of the tholeiites could be primarily peridotite with small amounts of pyroxenite transformed from recycled gabbro with a minor amount of sediment. This is distinct from the pyroxenite of metasomatic-origin formed more recently in the source of the alkali basalts.

As illustrated in Fig. 10, although the isotopic composition of melt inclusions hosted by olivine in tholeiites varies considerably, there is limited variation in the major and minor element composition of both the melt inclusions and host olivine. This suggests that the isotopic composition of mantle source rocks was strongly influenced by the addition of a small amount of a distinct source component while major element compositions were largely unaffected. Previous isotopic modeling showed that even a small amount of sediment incorporated into the mantle source would have a significant impact on isotopic composition (Hofmann, 1997; Rehkamper and Hofmann, 1997; Eisele et al., 2002; Murphy et al., 2002). Therefore, recycled ancient oceanic crust and sediment would be suitable candidates for the EM1-like signature of the Cenozoic basalts in the NCC.

### 5.5. Mantle source heterogeneity and implications for lithospheric evolution

The melt inclusion data from Hannuoba, combined with whole rock geochemical data can be used to place constraints on the time scale and spatial distribution of the compositional heterogeneity within the mantle source of the Cenozoic Hannuoba basalts. Generally, the compositions of the melt inclusions in most of the olivine grains from alkali and tholeiitic basalts are similar to those of whole rocks (Fig. 2, 5). The major element and Pb isotopic compositions of only three melt inclusions in the alkali basalts differ from those of the whole rocks (Fig. 2, 5). This exotic melt fraction is small in volume (~2%) and is therefore readily obscured in bulk rock compositions that were formed by mixing processes.

It is well documented that the NCC underwent considerable lithospheric thinning (Gao et al., 2004; Reisberg et al., 2005; Wu et al., 2005; Zhang, 2005). However, the timing and duration of the lithospheric thinning in the NCC remains a matter of hot debate (Xu et al., 2009). The shift from alkali basalt to tholeiite in the western NCC during the Cenozoic was used to infer the progressive lithospheric thinning, whereas the reverse trend in the eastern NCC was employed to imply

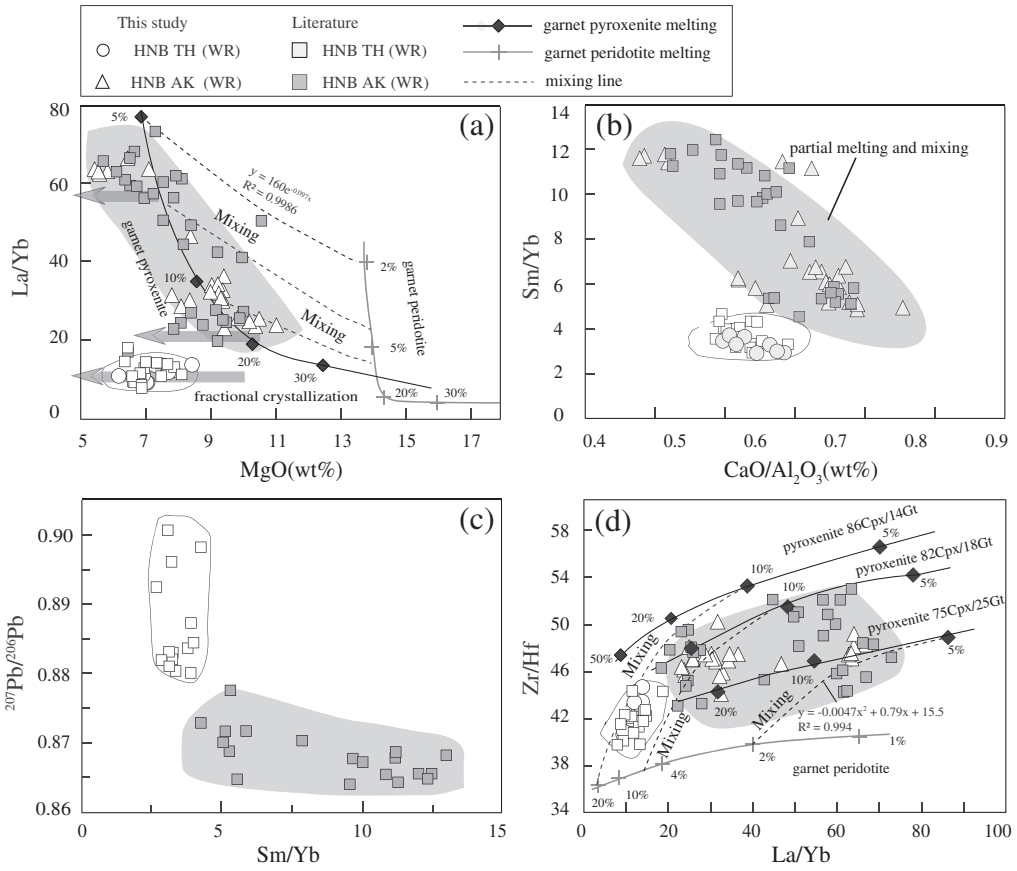


**Fig. 8.** (a) The negative correlation between MgO and La/Yb in the alkali basalts. (b) Sm/Yb versus $CaO/Al_2O_3$, showing the negative correlation between them in the alkali basalts; the tholeiites show a limited range of $CaO/Al_2O_3$ and Sm/Yb; (c) Sm/Yb versus $^{207}Pb/^{206}Pb$; the tholeiites have a large range of $^{207}Pb/^{206}Pb$ and a constant Sm/Yb, while the alkali basalts have an almost constant $^{207}Pb/^{206}Pb$; (d) variations in La/Yb vs. Zr/Hf. The melting curves for garnet pyroxenite are calculated by using the non-modal batch melting model. The black diamonds denote partial melts of garnet pyroxenite with different clinopyroxene (cpx)/garnet (gt) ratios: the partition coefficients of La and Yb for different minerals are from Hauri et al. (1994) and Johnson (1994); the partition coefficients of Zr and Hf for different minerals are from Pertermann et al. (2004); the partition coefficients of MgO for cpx and gt are from Takahashi (1986) and Kogiso et al. (2003), respectively. The compositions of garnet pyroxenite (silica-deficient pyroxenite) are from Lambart et al. (2013). The batch melting curve of garnet peridotite (gray cross) is calculated using the partition coefficients of La, Yb, Zr and Hf for different minerals from Timm et al. (2010); the MgO contents of garnet–peridotite melts are from Kushiro (1996), respectively. The melt fraction is displayed as a percent along the melting curves. The symbols for the Hannuoba basalts are the same as in Fig. 2.

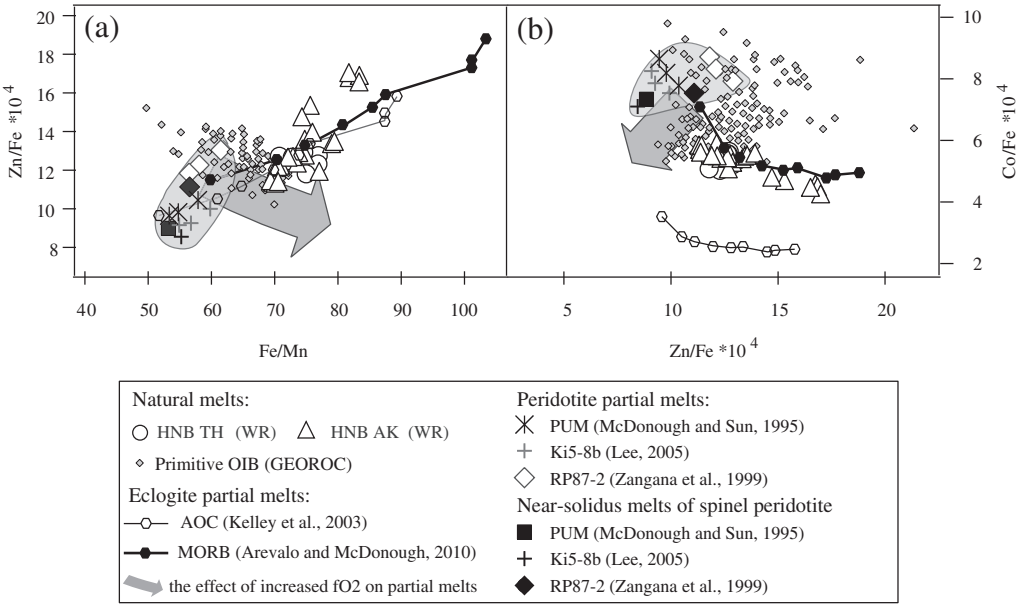


**Fig. 9.** (a–b) Zn/Fe, Co/Fe and Fe/Mn ratios for the Hannuoba basalts and partial melts of pyroxenite and peridotite. Experimental melts of pyroxenite and peridotite (McDonough and Sun, 1995; Zangana et al., 1999; Kelley et al., 2003; Lee, 2005; Arevalo and McDonough, 2010) are shown for reference. Primitive OIBs having MgO > 10% and < 20% are modified after Davis et al. (2013). Gray arrows indicating inferred effect of increased $fO_2$ during partial melting are modified after Davis et al. (2013).

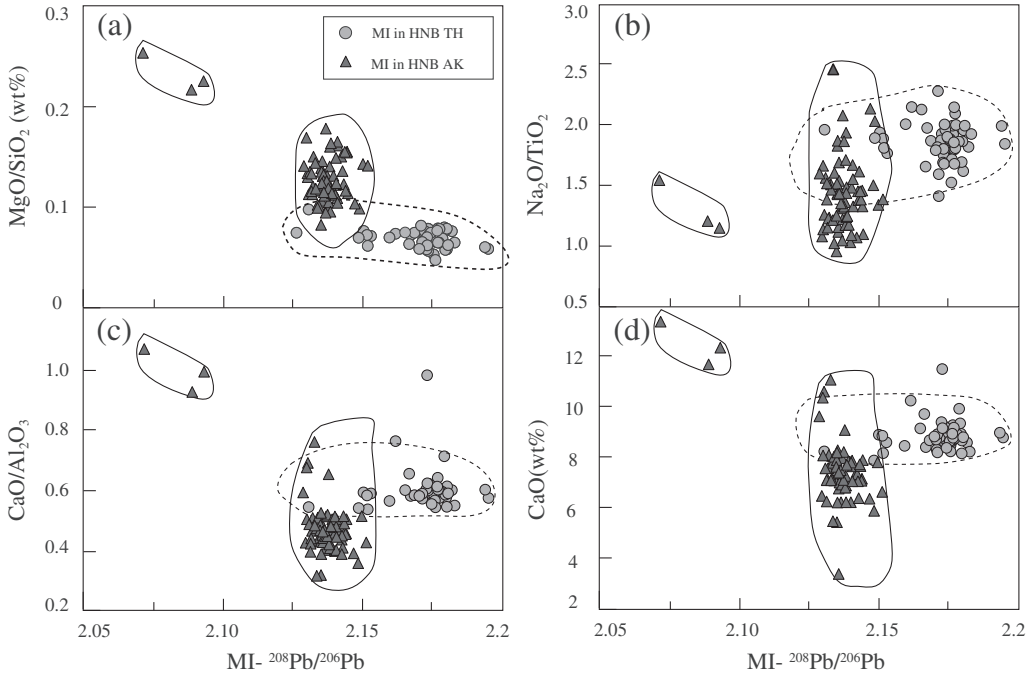


**Fig. 10.** (a–d) Major element compositions vs. $^{208}Pb/^{206}Pb$ for olivine-hosted melt inclusions in the Hannuoba tholeiitic and alkali basalts. Although the isotopic compositions of olivine-hosted melt inclusions in the tholeiites vary considerably, there is limited variation in the major element compositions of the melt inclusions. The Pb isotopic data for alkali basalt MI are roughly constant, except for three olivine-hosted melt inclusions, despite the large variations in major element composition of the melt inclusions.

lithospheric thickening during the Cenozoic (Xu et al., 2009). It is unlikely, however, that the interlayered association of alkali and tholeiitic basalts in Hannuoba is accompanied by variations in lithospheric thickness over a narrow interval of time. The different trace elemental and isotopic compositions of alkali and tholeiitic basalts could instead reflect source heterogeneity, rather than variations in the lithospheric thickness. Both alkaline and tholeiitic basaltic compositions have also been found in melt inclusions from alkali basalt in the Shanwang region, Shandong province (our unpublished data), where only alkali basalts have been erupted. This suggests that mantle source characteristics should be better understood before whole rock data are used to further constrain the history of lithospheric evolution in this region.

Recently, a low-velocity anomaly was observed beneath the Taihang region within the central zone of the NCC (An et al., 2009), implying a deep mantle plume origin of the Hannuoba basalts. The presence of recycled oceanic crust in the mantle source of Hannuoba tholeiitic basalts also supports a plume model. A FOZO-like component, generally thought to be derived from the lower mantle (Hauri et al., 1994), involved in the petrogenesis of Cenozoic basalts in the NCC is consistent with the presence of a deep-seated plume. The voluminous and widespread nature of basaltic volcanism (dominantly tholeiitic basalts) in the Hannuoba area and surrounding regions including the Jining, Chifeng and Abaga basalt provinces can therefore be related to extensive melting of the plume, particularly as geophysical evidence has confirmed that the lithosphere thickness beneath these areas is in excess of 100 km (Chen, 2010). A recent high-resolution tomographic model reveals a significantly Y-shaped hot anomaly under the central NCC extending down to the lower mantle, which suggests the possibility of a mantle plume beneath the region (Lei et al., 2013). Consequently, the voluminous and widespread basaltic volcanism in the Hannuoba region can be best explained by a plume model.

## 6. Conclusions

Our data, together with previously published isotopic data suggest that the limited Pb isotopic variation, coupled with the wide range of major and trace element compositions of the alkali suite, can be attributed to partial melting of garnet–pyroxenite and peridotite. Alkali basalts with relatively low MgO content and high La/Yb and Zr/Hf may have been generated from partial melting of the dominant garnet–pyroxenite, while alkali basalts with high MgO content and low La/Yb and Zr/Hf are consistent with a greater input from a garnet peridotite source. The pyroxenite involved in the formation of the alkali basalts may be located in the lithosphere and be of recent metasomatic origin.

The wide range of isotopic composition of the tholeiitic basalts, which have remarkably limited variation in major element composition, is argued to reflect their source region characteristics. The source lithology for the tholeiites is a mixture of peridotite with small amounts of garnet pyroxenite transformed from recycled ancient oceanic crust and sediment. The Pb isotopic compositions of the tholeiitic melt inclusions, which extend toward EM1-like values, may have been derived from recycled ancient oceanic crust and sediment. The presence of recycled oceanic crust in the mantle source and the low-velocity anomaly observed beneath the Taihang Mountains, located 50 km to the southeast of the Hannuoba region, support a plume model for this region.

Supplementary data to this article can be found online at http://dx.doi.org/10.1016/j.chemgeo.2015.02.018.

## Acknowledgments

We thank Lei Wu, Yin Liu and Xiang-lin Tu for technical assistance during the melt inclusion pretreatment and major and trace element analysis. We thank Prof. Yi-Gang Xu for comments and suggestions. We thank Dr. Richard Wysoczanski for improving the English. The paper benefited from helpful comments on an earlier version of the manuscript from Vadim Kamenetsky. We acknowledge the Editor Laurie Reisberg and Vadim Kamenetsky and two anonymous reviewers for their constructive comments which have greatly improved the manuscript. Financial support from the National Natural Science Foundation of China (91214202; 91014007; 90714001) and the "hundred talent project" of the Chinese Academy of Sciences is gratefully acknowledged. This is contribution No. 2010 from GIG-CAS.

## References


An, M., Feng, M., Zhao, Y., 2009. Destruction of lithosphere within the north China craton inferred from surface wave tomography. Geochem. Geophys. Geosyst. 10, Q08016. http://dx.doi.org/10.1029/2009GC002562.

Arevalo, R., McDonough, W.F., 2010. Chemical variations and regional diversity observed in MORB. Chem. Geol. 271, 70–85.

Arndt, N.T., Goldstein, S.L., 1989. An open boundary between lower continental crust and mantle: its role in crust formation and crustal recycling. Tectonophysics 161, 201–212.

Basu, A.R., Wang, J., Huang, W., Xie, G., Tatsumoto, M., 1991. Major element, REE, and Pb, Nd and Sr isotopic geochemistry of Cenozoic volcanic rocks of eastern China: implications for their origin from suboceanic-type mantle reservoirs. Earth Planet. Sci. Lett. 105, 149–169.

Chen, L., 2010. Concordant structural variations from the surface to the base of the upper mantle in the North China Craton and its tectonic implications. Lithos 120, 96–115.

Chen, L.H., Zeng, G., Jiang, S.Y., Hofmann, A.W., Xu, X.S., Pan, M.B., 2009. Sources of Anfengshan basalts: subducted lower crust in the Sulu UHP belt, China. Earth Planet. Sci. Lett. 286, 426–435.

Choi, S.H., Mukasa, S.B., Zhou, X.H., Xian, X.H., Andronikov, A.V., 2008. Mantle dynamics beneath East Asia constrained by Sr, Nd, Pb and Hf isotopic systematics of ultramafic xenoliths and their host basalts from Hannuoba, North China. Chem. Geol. 248, 40–61.

Class, C., Goldstein, S.L., 1997. Plume–lithosphere interaction in the ocean basins: contraints from source mineralogy. Earth Planet. Sci. Lett. 150, 245–260.

Danyushevsky, L.V., Della-Pasqua, F.N., Sokolov, S., 2000. Re-equilibration of melt inclusions trapped by magnesian olivine phenocrysts from subduction-related magmas: petrological implications. Contrib. Mineral. Petrol. 138, 68–83.

Davis, F.A., Humayun, M., Hirschmann, M.M., Cooper, R.S., 2013. Experimentally determined mineral/melt partitioning of first-row transition elements (FRTE) during partial melting of peridotite at 3 GPa. Geochim. Cosmochim. Acta 104, 232–260.

Eisele, J., Sharma, M., Galer, S.J.G., Blichert-Toft, J., Devey, C.W., Hofmann, A.W., 2002. The role of sediment recycling in EM-1 inferred from Os, Pb, Hf, Nd, Sr isotope and trace element systematics of the Pitcairn hotspot. Earth Planet. Sci. Lett. 196, 197–212.

Farmer, G.L., 2003. Continental basaltic rocks. Treatise Geochem. 3, 85–121.
Foley, S.F., Barth, M.G., Jenner, G.A., 2000. Rutile/melt partition coefficients for trace elements and an assessment of the influence of rutile on the trace element characteristics of subduction zone magmas. Geochim. Cosmochim. Acta 64, 933–938.

Foley, S.F., Jackson, S.E., Fryer, B.J., Greenough, J.D., Jenner, G.A., 1996. Trace element partition coefficients for clinopyroxene and phlogopite in an alkaline lamprophyre from Newfoundland by LAM-ICP-MS. Geochim. Cosmochim. Acta 60, 629–638.

Ford, C.E., Russell, D.G., Cracen, J.A., Fisk, M.R., 1983. Olivine–liquid equilibria: temperature, pressure and composition dependence of the crystal/liquid cation partition coefficients for Mg, $Fe^{2+}$, Ca and Mn. J. Petrol. 24, 256–266.

Gao, S., Rudnick, R.L., Yuan, H.-L., Liu, X.-M., Liu, Y.-S., Xu, W.-L., Ling, W.-L., Ayers, J., Wang, X.-C., Wang, Q.-H., 2004. Recycling lower continental crust in the North China Craton. Nature 432, 892–897.

Goto, A., Tatsumi, Y., 1996. Quantitative analyses of rock samples by an X-ray fluorescence spectrometer (II). Rigaku J. 13, 20–39.

Gurenko, A.A., Chaussidona, M., 1995. Enriched and depleted primitive melts included in olivine from Icelandic tholeiites: origin by continuous melting of a single mantle column. Geochim. Cosmochim. Acta 59, 2905–2917.

Gurenko, A.A., Sobolev, A.V., Hoernle, K.A., Hauff, F., Schmincke, H.U., 2009. Enriched, HIMU-type peridotite and depleted recycled pyroxenite in the Canary plume: A mixed-up mantle. Earth Planet. Sci. Lett. 277, 514–524.

Hart, S.R., Hauri, E.H., Oschmann, L.A., Whitehead, J.A., 1992. Mantle plumes and entrainment: isotopic evidence. Science 256, 517–520.

Hauri, E.H., Whitehead, J.A., Hart, S.R., 1994. Fluid dynamic and geochemical aspects of entrainment in mantle plumes. J. Geophys. Res. 99, 24275–24300.

Herzberg, C., Cabral, R.A., Jackson, M.G., Vidito, C., Day, J.M.D., Hauri, E.H., 2014. Phantom Archean crust in Mangaia hot spot lavas and the meaning of heterogeneous mantle. Earth Planet. Sci. Lett. 396, 97–106.

Hirschmann, M.M., Kogiso, T., Baker, M.B., Stolper, E.M., 2003. Alkalic magmas generated by partial melting of garnet pyroxenite. Geology 31, 481–484.

Ho, K.S., Liu, Y., Chen, J.C., Yang, H.J., 2008. Elemental and Sr–Nd–Pb isotopic compositions of late Cenozoic Abaga basalts, Inner Mongolia: Implications for petrogenesis and mantle process. Geochem. J. 42, 339–357.

Hofmann, A.W., 1997. Mantle geochemistry: the message from oceanic volcanism. Nature 385, 219–229.

Hofmann, A.W., Jochum, K.P., Seufert, M., White, W.M., 1986. Nb and Pb in oceanic basalts: new constraints on mantle evolution. Earth Planet. Sci. Lett. 79, 33–45.

Hong, L.B., Zhang, Y.H., Qian, S.P., Liu, J.Q., Ren, Z.Y., Xu, Y.G., 2013. Constraints from melt inclusions and their host olivines on the petrogenesis of Oligocene–Early Miocene Xindian basalts, Chifeng area, North China Craton. Contrib. Mineral. Petrol. 165, 305–326.

Johnson, K.T.M., 1994. Experimental cpx/and garnet/melt partitioning of REE and other trace elements at high pressures; petrogenetic implications. Mineral. Mag. 58, 454–455.

Jull, M., Kelemen, P.B., 2001. On the conditions for lower crustal convective instability. J. Geophys. Res. 106, 6423–6446.

Kamenetsky, V.S., Elburg, M., Arculus, R., Thomas, R., 2006. Magmatic origin of low-Ca olivine in subduction-related magmas: Co-existence of contrasting magmas. Chem. Geol. 233, 346–357.

Kamenetsky, V.S., Chung, S.L., Kamenetsky, M.B., Kuzmin, D.V., 2012. Picrites from the Emeishan large igneous province, SW China: a compositional continuum in primitive magmas and their Respective Mantle Sources. J. Petrol. 53, 2095–2113.

Kelley, K.A., Plank, T., Ludden, J., Staudigel, H., 2003. Composition of altered oceanic crust at ODP Sites 801 and 1149. Geochem. Geophys. Geosyst. 4.

Kogiso, T., Hirschmann, M.M., Frost, D.J., 2003. High-pressure partial melting of garnet pyroxenite: possible mafic lithologies in the source of ocean island basalts. Earth Planet. Sci. Lett. 216, 603–617.

Kushiro, I., 1996. Earth processes: Reading the isotopic code. In: Basu, A., Hart, S. (Eds.), Geophysical Monograph, American Geophysical Union 95, pp. 109–122.

Lambart, S., Laporte, D., Schiano, P., 2013. Markers of the pyroxenite contribution in the major-element compositions of oceanic basalts: overview of the experimental constraints. Lithos 160–161, 14–36.

LaTourrette, T., Hervig, R.L., Holloway, J.R., 1995. Trace element partitioning between amphibole, phlogopite, and basanite melt. Earth Planet. Sci. Lett. 135, 13–30.

Le Bas, M.J., Lemaitre, R.W., Streckeisen, A., Zanettin, B., 1986. A chemical classification of volcanic-rocks based on the total alkali silica diagram. J. Petrol. 27, 745–750.

le Roex, A.P., Spath, A., Zartman, R.E., 2001. Lithospheric thickness beneath the southern Kenya Rift: implications from basalt geochemistry. Contrib. Mineral. Petrol. 142, 86–106.

Le Roux, V., Dasgupta, R., Lee, C.T.A., 2011. Mineralogical heterogeneities in the Earth's mantle: Constraints from Mn, Co, Ni and Zn partitioning during partial melting. Earth Planet. Sci. Lett. 307, 395–408.

Lei, J.S., Xie, F.R., Fan, Q.C., Santosh, M., 2013. Seismic imaging of the deep structure under the Chinese volcanoes: An overview. Phys. Earth Planet. Inter. 224, 104–123.

Lee, C.T.A., 2005. Trace element evidence for hydrous metasomatism at the base of the North American lithosphere and possible association with Laramide low-angle subduction. J. Geol. 113, 673–685.

Liu, R.X., 1992. Geochronology and geochemistry of the Cenozoic volcanics in China. Seismological Press (in Chinese), Beijing.

Liu, D.Y., Nutman, A.P., Compston, W., Wu, J.S., Shen, Q.H., 1992. Remnants of greater than or equal to 3800 Ma crust in the Chinese part of the Sino-Korean Craton. Geology 20, 339–342.

Liu, Y., Liu, H.C., Li, X.H., 1996. Simultaneous and precise determination of 40 trace elements in rock samples using ICP-MS. Geochimica 25, 552–558 (in Chinese with English abstract).

Liu, Y.S., Gao, S., Kelemen, P.B., Xu, W.L., 2008. Recycled crust controls contrasting source compositions of Mesozoic and Cenozoic basalts in the North China Craton. Geochim. Cosmochim. Acta 72, 2349–2376.

Lustrino, M., 2005. How the delamination and detachment of lower crust can influence basaltic magmatism. Earth-Sci. Rev. 72, 21–38.

Macdonald, G.A., Katsura, T., 1964. Chemical composition of Hawaiian lavas. J. Petrol. 5, 82–133.

Maclennan, J., 2008. Lead isotope variability in olivine-hosted melt inclusions from Iceland. Geochim. Cosmochim. Acta 72, 4159–4176.

McDonough, W.F., Sun, S.S., 1995. The composition of the Earth. Chem. Geol. 120, 223–253.

Médard, E., Schmidt, M.W., Schiano, P., Ottolini, L., 2006. Melting of amphibole-bearing wehrlites: an experimental study on the origin of ultra-calcic nepheline-normative melts. J. Petrol. 47, 481–504.

Menzies, M.A., Fan, W.M., Zhang, M., 1993. Palaeozoic and Cenozoic lithoprobes and the loss of >120km of Archaean lithosphere, Sino-Korean craton, China. In: Prichard, H.M., Alabaster, T., Harris, N.B.W., Neary, C.R. (Eds.), Magmatic Processes and Plate Tectonics.London: Geol. Soc. Spe. Pub. 76, pp. 71–78

Murphy, D.T., Collerson, K.D., Kamber, B.S., 2002. Lamproites from Gaussberg, Antarctica: Possible transition zone melts of Archaean subducted sediments. J. Petrol. 43, 981–1001.

Niu, Y., O'Hara, M.J., 2003. Origin of ocean island basalts: A new perspective from petrology, geochemistry, and mineral physics considerations. J. Geophys. Res. 108, 2209. http://dx.doi.org/10.1029/2002JB002048.

Pertermann, M., Hirschmann, M.M., Hametner, K., Gu¨nther, D., Schmidt, M.W., 2004. Experimental determination of trace element partitioning between garnet and silica-rich liquid during anhydrous partial melting of MORB-like eclogite. Geochem. Geophys. Geosyst. 5. http://dx.doi.org/10.1029/2003GC000638.

Pilet, S., Baker, M.B., Stolper, E.M., 2008. Metasomatized lithosphere and the origin of alkaline lavas. Science 320, 916–919.

Pilet, S., Baker, M.B., Muntener, O., Stolper, E.M., 2011. Monte Carlo simulations of metasomatic enrichment in the lithosphere and implications for the source of alkaline basalts. J. Petrol. 52, 1415–1442.

Rapp, R.P., Irifune, T., Shimizu, N., Nishiyama, N., Norman, M.D., Inoue, J., 2008. Subduction recycling of continental sediments and the origin of geochemically enriched reservoirs in the deep mantle. Earth Planet. Sci. Lett. 271, 14–23.

Rehkamper, M., Hofmann, A.W., 1997. Recycled ocean crust and sediment in Indian Ocean MORB. Earth Planet. Sci. Lett. 147, 93–106.

Reisberg, L., Zhi, X.C., Lorand, J.P., Wagner, C., Peng, Z.C., Zimmermann, C., 2005. Re–Os and S systematics of spinel peridotite xenoliths from east central China: Evidence for contrasting effects of melt percolation. Earth Planet. Sci. Lett. 239, 286–308.

Ren, Z.Y., Takahashi, E., Orihashi, Y., Johnson, K.T.M., 2004. Petrogenesis of tholeiitic lavas from the submarine Hana Ridge, Haleakala Volcano, Hawaii. J. Petrol. 45, 2067–2099.

Ren, Z.Y., Ingle, S., Takahashi, E., Hirano, N., Hirata, T., 2005. The chemical structure of the Hawaiian mantle plume. Nature 436, 837–840.

Ren, Z.Y., Shibata, T., Yoshikawa, M., Johnson, K.T.M., Takahashi, E., 2006. Isotope compositions of submarine Hana Ridge lavas, Haleakala Volcano, Hawaii: implications for source compositions, melting process and the structure of the Hawaiian plume. J. Petrol. 47, 255–275.

Ren, Z.Y., Hanyu, T., Miyazaki, T., Chang, Q., Kawabata, H., Takahashi, T., Hirahara, Y., Nichols, R.L., Tatsumi, Y., 2009. Geochemical differences of the Hawaiian shield lavas: implications for melting process in the heterogeneous Hawaiian Plume. J. Petrol. 50, 1553–1573.

Roeder, P.L., Emslie, R.F., 1970. Olivine–liquid equilibrium. Contrib. Mineral. Petrol. 29, 275–289.
Rosenbaum, J.M., 1993. Mantle phlogopite: a significant lead repository. Chem. Geol. 106, 457–483.
Rudnick, R.L., Gao, S., 2003. Composition of the continental crust. In: Carlson, R.W. (Ed.), Treatise on Geochemistry 3, The mantle and core. Elsevier, New York, pp. 1–70.
Rudnick, R.L., Gao, S., Ling, W.L., Liu, Y.S., McDonough, W.F., 2004. Petrology and geochemistry of spinel peridotite xenoliths from Hannuoba and Qixia, North China Craton. Lithos 77, 609–637.
Saal, A.E., Hart, S., Shimizu, N., Hauri, E., Layne, G., Eiler, J., 1998. Pb isotopic variability in melt inclusions from oceanic island basalts, Polynesia. Science 282, 1481–1484.
Saal, A., Hart, S., Shimizu, N., Hauri, E., Layne, G., Eiler, J., 2005. Pb isotopic variability in melt inclusions from the EMI–EMII–HIMU mantle end-members and the role of the oceanic lithosphere. Earth Planet. Sci. Lett. 240, 605–620.
Sakuyama, T., Tian, Wei, Kimura, J.I., Fukao, Y., Hirahara, Y., Toshiro, T., Senda, R., Chang, Q., Miyazaki, T., Obayashi, M., Kawabata, H., Tatsumi, Y., 2013. Melting of dehydrated oceanic crust from the stagnant slab and of the hydrated mantle transition zone: Constraints from Cenozoic alkaline basalts in eastern China. Chem. Geol. 35, 932–948.
Sato, H., 1977. Nickel content of basaltic magmas: identification of primary magmas and a measure of the degree of olivine fractionation. Lithos 10, 113–120.
Sobolev, A.V., Chaussidon, M., 1996. $H_2O$ concentrations in primary melts from supra-subduction zones and mid-ocean ridges: Implications for $H_2O$ storage and recycling in the mantle. Earth Planet. Sci. Lett. 137, 45–55.
Sobolev, A.V., Shimizu, N., 1993. Ultra-depleted primary melt included in an olivine from the Mid-Atlantic Ridge. Nature 363, 151–154.
Sobolev, A.V., Hofmann, A.W., Nikogosian, I.K., 2000. Recycled oceanic crust observed in 'ghost plagioclase' within the source of Mauna Loa lavas. Nature 404, 986–990.
Sobolev, A.V., Hofmann, A.W., Sobolev, S.V., Nikogosian, I.K., 2005. An olivine-free mantle source of Hawaiian shield basalts. Nature 434, 590–597.
Sobolev, A.V., Hofmann, A.W., Kuzmin, D.V., Yaxley, G.M., Arndt, N.T., Chung, S.-L., Danyushevsky, L.V., Elliott, T., Frey, F.A., Garcia, M.O., Gurenko, A.A., Kamenetsky, V.S., Kerr, A.C., Krivolutskaya, N.A., Matvienkov, V.V., Nikogosian, I.K., Rocholl, A., Sigurdsson, I.A., Sushchevskaya, N.M., Teklay, M., 2007. The amount of recycled crust in sources of mantle-derived melts. Science 316, 412–417.
Song, Y., Frey, F.A., Zhi, X.C., 1990. Isotopic characteristics of Hannuoba basalts, Eastern China: implications for their petrogenesis and the composition of subcontinental mantle. Chem. Geol. 88, 35–52.
Sorbadere, F., Schiano, P., Métrich, N., 2013. Constraints on the origin of nepheline-normative primitive magmas in island arcs inferred from olivine-hosted melt inclusion compositions. J. Petrol. 54, 215–233.
Stracke, A., Bizimis, M., Salters, V.J.M., 2003. Recycling oceanic crust: quantitative constraints. Geochem. Geophys. Geosyst. 4. http://dx.doi.org/10.1029/2001GC000223.
Sun, S.S., McDonough, W.F., 1989. Chemical and isotopic systematics of oceanic basalts: implications for mantle composition and processes. In: Saunders, A.D., Norry, M.J. (Eds.), Magmatism in the ocean basins. London: Geological Society Special Publicaiton 42, pp. 313–345.
Takahashi, E., 1986. Melting of a dry peridotite KLB-1 up to 14 GPa-implications on the origin of peridotitic upper mantle. J. Geophys. Res. 91, 9367–9382.
Tang, Y.J., Zhang, H.F., Ying, J.F., 2006. Asthenosphere–lithospheric mantle interaction in an extensional regime: Implication from the geochemistry of Cenozoic basalts from Taihang Mountains, North China Craton. Chem. Geol. 233, 309–327.
Tang, Y.J., Zhang, H.F., Nakamura, E., Moriguti, T., Kobayashi, K., Ying, J.F., 2007. Lithium isotopic systematics of peridotite xenoliths from Hannuoba, North China Craton: Implications for melt–rock interaction in the considerably thinned lithospheric mantle. Geochim. Cosmochim. Acta 71, 4327–4341.
Tang, Y.J., Zhang, H.F., Ying, J.F., Zhang, J., Liu, X.M., 2008. Refertilization of ancient lithospheric mantle beneath the central North China Craton: Evidence from petrology and geochemistry of peridotite xenoliths. Lithos 101, 435–452.
Tang, Y.J., Zhang, H.F., Ying, J.F., Su, B.X., Chu, Z.Y., Xiao, Y., Zhao, X.M., 2013. Highly heterogeneous lithospheric mantle beneath the Central Zone of the North China Craton evolved from Archean mantle through diverse melt refertilization. Gondwana Res. 23, 130–140.
Thirlwall, M.F., 1997. Pb isotopic and elemental evidence for OIB derivation from young HIMU mantle. Chem. Geol. 139, 51–74.
Thompson, R.N., Gibson, S.A., 2000. Transient high temperatures in mantle plume heads inferred from magnesian olivines in Phanerozoic picrites. Nature 407, 502–506.
Timm, C., Hoernle, K., Werner, R., Hauff, F., den Bogaard, P.V., White, J., Mortimer, N., Garbe-Schönberg, D., 2010. Temporal and geochemical evolution of the Cenozoic intraplate volcanism of Zealandia. Earth-Sci. Rev. 98, 38–64.
Ulmer, P., 1989. The dependence of Fe–Mg cation-partitioning between olivine and basaltic liquid on pressure, temperature and composition. Contrib. Mineral. Petrol. 101, 261–273.
Wang, Y., Zhao, Z.F., Zheng, Y.F., Zhang, J.-J., 2011. Geochemical constraints on the nature of mantle source for Cenozoic continental basalts in east-central China. Lithos 125, 940–955.
Wang, Z., Gaetani, G.A., Zheng, Y.F., Zhang, J.-J., 2008. artitioning of Ni between olivine and siliceous ecloge partial melt: experimental constraints on the mantle source of Hawaiian basalts. Contrib.Mineral.Petrol 156, 661–678.
Workman, R.K., Hart, S.R., Jackson, M., Regelous, M., Farley, K., Blusztajn, A.J., Kurz, M., Staudigel, H., 2004. Recycled metasomatized lithosphere as the origin of the Enriched Mantle II (EM2) end-member: Evidence from the Samoan Volcanic Chain. Geochem. Geophys. Geosyst. 5, Q04008. http://dx.doi.org/10.1029/2003GC000623.
Wu, F.Y., Lin, J.Q., Wilde, S.A., Zhang, X.O., Yang, J.H., 2005. Nature and significance of the early Cretaceous giant igneous event in eastern China. Earth Planet. Sci. Lett. 233, 103–119.
Xu, Y.G., 2001. Thermo-tectonic destruction of the archaean lithospheric keel beneath the Sino-Korean Craton in China: Evidence, timing and mechanism. Phys. Chem. Earth Solid Earth Geod. 26, 747–757.
Xu, Y.G., Ma, J.L., Frey, F.A., Feigenson, M.D., Liu, J.F., 2005. Role of lithosphere–asthenosphere interaction in the genesis of Quaternary alkali and tholeiitic basalts from Datong, western North China Craton. Chem. Geol. 224, 247–271.
Xu, Y.G., Li, H.Y., Pang, C.J., He, B., 2009. On the timing and duration of the destruction of the North China Craton. Chin. Sci. Bull. 54, 3379–3396.
Xu, Y.G., Zhang, H.H., Qiu, H.N., Ge, W.C., Wu, F.Y., 2012a. Oceanic crust components in continental basalts from Shuangliao, Northeast China: Derived from the mantle transition zone? Chem. Geol. 328, 168–184.
Xu, Z., Zhao, Z.F., Zheng, Y.F., 2012b. Slab–mantle interaction for thinning of cratonic lithospheric mantle in North China: Geochemical evidence from Cenozoic continental basalts in central Shandong. Lithos 147, 202–217.
Yaxley, G.M., Sobolev, A.V., 2007. High-pressure partial melting of gabbro and its role in the Hawaiian magma source. Contrib. Mineral. Petrol. 154, 371–383.
Zangana, N.A., Downes, H., Thirlwall, M.F., Marriner, G.F., Bea, F., 1999. Geochemical variation in peridotite xenoliths and their constituent clinopyroxenes from Ray Pic (French Massif Central): implications for the composition of the shallow lithospheric mantle. Chem. Geol. 153, 11–35.
Zeng, G., Chen, L.-H., Xu, X.S., Jiang, S.Y., Hofmann, A.W., 2010. Carbonated mantle sources for Cenozoic intra-plate alkaline basalts in Shandong, North China. Chem. Geol. 273, 35–45.
Zeng, G., Chen, L.-H., Hofmann, A.W., Jiang, S.-Y., Xu, X.-S., 2011. Crust recycling in the sources of two parallel volcanic chains in Shandong, North China. Earth Planet. Sci. Lett. 302, 359–368.
Zhang, H.F., 2005. Transformation of lithospheric mantle through peridotite–melt reaction: A case of Sino-Korean craton. Earth Planet. Sci. Lett. 237, 768–780.
Zhang, H.F., Sun, M., Zhou, X.H., Zhou, M.F., Fan, W.M., Zheng, J.P., 2003. Secular evolution of the lithosphere beneath the eastern North China Craton: evidence from Mesozoic basalts and high-Mg andesites. Geochim. Cosmochim. Acta 67, 4373–4387.
Zhang, J.J., Zheng, Y.F., Zhao, Z.F., 2009. Geochemical evidence for interaction between oceanic crust and lithospheric mantle in the origin of Cenozoic continental basalts in east-central China. Lithos 110, 305–326.
Zhang, W.H., Zhang, H.F., Fan, W.M., Han, B.F., Zhou, M.F., 2012. The genesis of Cenozoic basalts from the Jining area, northern China: Sr–Nd–Pb–Hf isotope evidence. J. Asian Earth Sci. 61, 128–142.
Zhang, L., Ren, Z.Y., Nichols, A.R.L., Zhang, Y.H., Zhang, Y., Qian, S.P., Liu, J.Q., 2014. Lead isotope analysis of melt inclusions by LA–MC–ICP-MS. J. Anal. At. Spectrom. 29, 1393–1405.
Zhao, G.C., Wilde, S.A., Cawood, P.A., Sun, M., 2001. Archean blocks and their boundaries in the North China Craton: lithological, geochemical, structural and P–T path constraints and tectonic evolution. Precambrian Res. 107, 45–73.
Zhi, X.C., Song, Y., Frey, F.A., Feng, J.L., Zhai, M.Z., 1990. Geochemistry of Hannuoba basalts, Eastern China: constraints on the origin of continental alkalic and tholeiitic Basalt. Chem. Geol. 88, 1–33.
Zindler, A., Hart, S., 1986. Chemical Geodynamics. Annu. Rev. Earth Planet. Sci. 14, 493–571.